Miner Petrol (2016) 110:247–268
DOI 10.1007/s00710-015-0388-0

ORIGINAL PAPER

Petrogenesis of Mesoproterozoic lamproite dykes from the Garledinne (Banganapalle) cluster, south-western Cuddapah Basin, southern India

N. V. Chalapathi Rao[1] · Atiullah[1] · Alok Kumar[1] · Samarendra Sahoo[1] · Purnendu Nanda[1] · Ngazimpi Chahong[1] · B. Lehmann[2] · K. V. S. Rao[3]

Received: 25 November 2014 / Accepted: 20 May 2015 / Published online: 12 June 2015

Abstract We report mineral chemistry and whole-rock major and trace-element geochemistry for a recent find of Mesoproterozoic (~1.4 Ga) lamproites from the Garledinne (Banganapalle) cluster, south-western part of the Paleo-Mesoproterozoic Cuddapah Basin, southern India. The Garledinne lamproites occur as WNW–ESE-trending dykes that have undergone varying degree of pervasive silicification and carbonate alteration. Nevertheless, their overall texture and relict mineralogy remain intact and provide important insights into the nature of their magmas. The lamproite dykes have porphyritic to weakly porphyritic textures comprising pseudomorphed olivine macrocrysts and microphenocrysts, titanian phlogopite microphenocrysts, spinel having a compositional range from chromite to rarely magnesiochromite, Sr-rich apatite and niobian rutile. The Garledinne and other Cuddapah Basin lamproites (Chelima and Zangamarajupalle) collectively lack sanidine, clinopyroxene, potassic richterite, and titanite and are thus mineralogically distinct from the nearby Mesoproterozoic lamproites (Krishna and Ramadugu) in the Eastern Dharwar Craton, southern India. The strong correlation between various major and trace elements coupled with high abundances of incompatible and compatible trace elements imply that alteration and crustal contamination have had a limited effect on the whole-rock geochemistry (apart from K_2O and CaO) of the Garledinne lamproites and that olivine fractionation played an important role in their evolution. The Garledinne lamproites represent small-degree partial melts derived from a refractory (previously melt extracted) peridotitic mantle source that was subsequently metasomatised (enriched) by carbonate–rich fluids/melts within the garnet stability field. The involvement of multiple reservoirs (sub-continental lithospheric mantle and asthenosphere) has been inferred in their genesis. The emplacement of the Garledinne lamproites is linked to extensional events, across the various Indian cratons, related to the break-up of the Proterozoic supercontinent of Columbia.

Re-Revised Paper submitted on 19.5.2015 to the *Mineralogy and Petrology* special issue dedicated to Late Professor Rex Prider

Editorial handling: P. Downes

✉ N. V. Chalapathi Rao
nvcr100@gmail.com

[1] Department of Geology, Centre of Advanced Study, Banaras Hindu University, Varanasi 221005, India

[2] Mineral Resources, Technical University of Clausthal, 38678 Clausthal-Zellerfeld, Germany

[3] De Beers India Exploration, 36/A, Peenya Industrial Area, II nd Phase, Bangalore 560058, India

Introduction

Precambrian lamproites are quite rare in the geological record compared to those recorded from the Phanerozoic. As a result, most of the current lamproite petrogenetic models are strongly influenced by studies on Phanerozoic lamproites (e.g., Leucite Hills, Smoky Butte, West Kimberley, Gaussberg, and the Mediterranean region; Murphy et al. 2002; Carlier and Lorand 2003; Coban and Flower 2006; Mirnejad and Bell 2006; Davies et al. 2006; Prelević et al. 2012). A significant number of Mesoproterozoic lamproites occur in the Eastern Dharwar, the Bastar and the Bundelkhand cratons of the Indian shield (Chalapathi Rao et al. 1996, 1999; Kumar et al. 2001; Osborne et al. 2011; Sahu et al. 2013) and they provide a unique opportunity to understand the tectono-magmatic processes when these cratons constituted a part of

Proterozoic supercontinents such as Columbia and Rodinia. Furthermore, the spatial association of Mesoproterozoic lamproites, some of which are diamondiferous, with two of the major Proterozoic Purāna sedimentary basins of peninsular India – the Vindhyan (Chalapathi Rao 2005 and references therein; Masun et al. 2009) in central India and the Cuddapah (Bergman 1987; Chalapathi Rao 2007) in southern India – remains one of the puzzling aspects of Indian geology. Of all these lamproite occurrences, only those from the Vindhyan Basin (Majhgawan, Hinota and Bunder) are diamondiferous whereas the lamproites from the Cuddapah Basin (Chelima and Zangamarajupalle) are non-diamondiferous (Geological Survey of India 2011). This scenario is intriguing since the gravels of the rivers Krishna and Tungabhadra (flowing through the Cuddapah Basin) and the Banganapalle Conglomerate horizon (belonging to the Kurnool Group of sedimentary rocks) within the Cuddapah Basin, have yielded the world-famous historical diamonds such as the Koh-I-Noor, Pitt, and Orloff implying that the primary source of these diamonds still remains elusive despite centuries of search (see Radhakrishna 2007 and the references therein).

Against this backdrop, De Beers India Exploration company has discovered lamproitic dykes intruding the Tadpatri shales of the Lower Cuddapah Supergroup, located west of Banganapalle town near Garledinne (Joy et al. 2012) in the south-western part of the Cuddapah Basin. Only reconnaissance petrological and geochemical information of these lamproite dykes is available and petrogenetic details are lacking. The Garledinne lamproite dykes thus offer an excellent opportunity to investigate the sub-continental lithospheric mantle (SCLM) in an entirely new geological domain within the SW part of the Cuddapah Basin. The major objectives of this paper are to: (i) document the detailed petrology and geochemistry of the Garledinne lamproite dykes so as to expand the available data set on such rocks from the Cuddapah Basin and the Eastern Dharwar Craton (EDC; Fig. 1a); (ii) compare the new data with those of the previously well-studied Chelima and Zangamarajupalle lamproites within the Cuddapah Basin (hence forth termed as Cuddapah lamproites) and the EDC lamproites (Krishna and Ramadugu lamproite fields) so as to decipher their similarities and differences; (iii) infer the petrogenesis of the Garledinne lamproite dykes; and (iv) better understand the geodynamic evolution of the SCLM beneath the Cuddapah Basin.

Geological setting and background information

The crescent-shaped Cuddapah Basin, covering an area of 44, 000 km^2 (Fig. 1a), is one of the largest of the Purāna (Holland 1907) Paleo- to Meso-Proterozoic sedimentary basins of India. It has been extensively studied for well over a century with regard to its structure, tectonics, igneous activity, sedimentation, stratigraphy, geochronology and mineral wealth (e.g., King 1872; Nagaraja Rao et al. 1987; Anand et al. 2003; Chetty 2011; Patranabis-Deb et al. 2012; Tripathy and Saha 2013; Basu and Bickford 2013; Bickford et al. 2013; Collins et al. 2014; Deb and Pal 2014). Despite these studies, the origin and evolution of the Cuddapah Basin still remains unclear with diverse models in vogue viz.: (i) Mesoproterozoic rifting (Chaudhuri et al. 2002); (ii) astrobleme impact (Krishna Brahmam and Dutt 1992); (iii) thermal subsidence (Bhattacharji and Singh 1984; Drury 1984; Mall et al. 2008); (iv) separation of the Napier Complex (presently in Antarctica) from the southern Indian block (Mohanty 2011); and (v) a peripheral foreland basin that evolved through continent-continent collision (Singh and Mishra 2002).

The Cuddapah Basin, with an estimated in-fill thickness of 12 km, contains rocks belonging to the Cuddapah Supergroup that is overlain by the younger Kurnool Group (Fig. 1a and b). The latter are hosted in two sub-basins - the Kurnool and Palnad basins (Fig. 1a). Extrusive as well as intrusive igneous rocks are present throughout the Cuddapah Supergroup with the exception of the uppermost Nallamalai Group. Extensive sub-aerial and submarine lava flows, pillow lavas, ash beds, ignimbrites, agglomerates, dykes and sills occur predominantly in the Vempalle Formation and to a lesser extent in the Tadpatri Formation along the SW fringes of the basin (Sen and Narasimha Rao 1971; Srikantia 1984; Chatterjee and Bhattacharjee 1998; Sesha Sai 2014). Most of the lavas are essentially basalt to trachy-basalt with very few being picrite (Anand et al. 2003; Mallikharjuna Rao et al. 2007). Minor lava flows, including rare spilitised basalts, are reported from the Tadpatri Formation (Reddy 1988) but no volcanic rocks are reported in the rocks younger than Tadpatri Formation. Intrusive rocks in the form of sills and dykes are present throughout the Lower Cuddapah formations and are mostly dolerite/gabbro, rarely picrite and a few are lamproite. The Cumbum Formation is intruded by lamproites at Chelima and Zangamarajupalle, and riebeckite-bearing alkali syenites at Racherla, Idamakallu and Giddalur (Fig. 1a; King 1872; Madhavan et al. 1994). The Kurnool Group is devoid of any igneous activity except for felsic (rhyolitic) tuff beds (Saha and Tripathy 2012) that have been recently re-interpreted to be volcaniclastic sandy mudstone (Bickford et al. 2013). A stratigraphic column of the Cuddapah Basin is provided in Fig. 1b with all available geochronological information.

Four sets of lamproite dykes, intruding the Tadpatri shales of the lower Cuddapah Supergroup, were reported by the De Beers Company in three areas near Banganapalle town: (i) in a road material quarry 4.5 km west, (ii) 1.7 km to the SW; and (iii) in a valley 24 km due west and exposed along a stream bed (Joy et al. 2012) near Garledinne village. In this study, we sampled a Garledinne lamproite dyke (15°18“27”N; 78° 00“8”E; Fig. 1c) that trends WNW-ESE and corresponds to the 188 551/110/

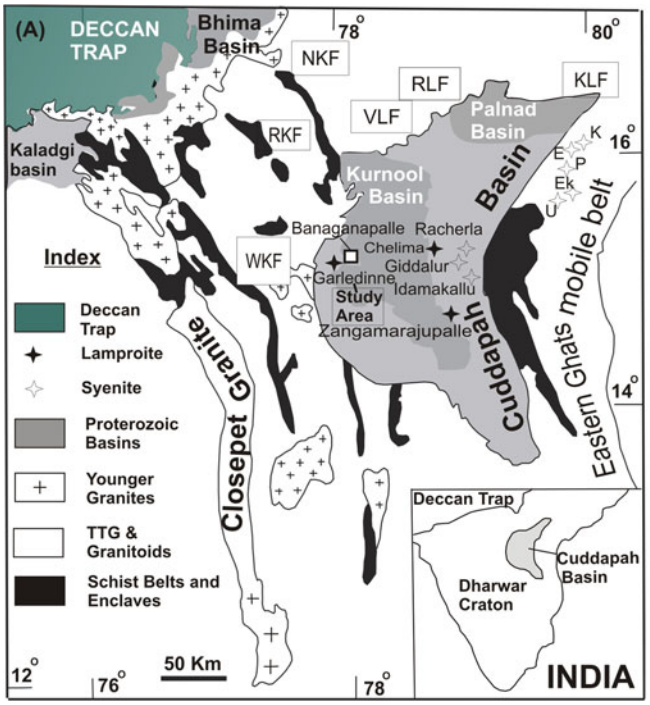

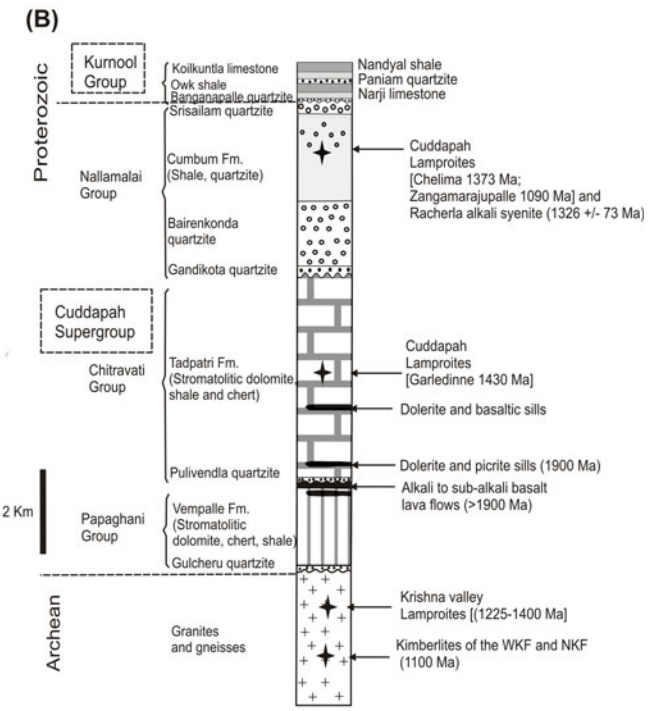

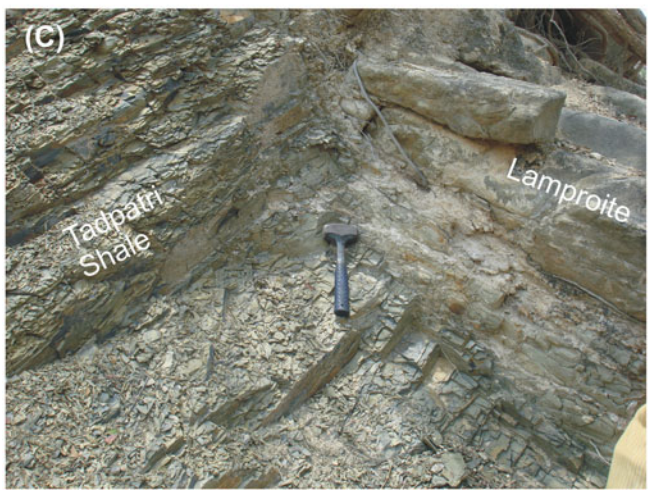

Fig. 1 **a** A generalised geological map of the Dharwar craton, southern India (after Naqvi and Rogers 1987) showing the Paleo-Mesoproterozoic Cuddapah basin and surrounding areas with the locations of kimberlite, lamproite and syenite occurrences. WKF= Wajrakarur kimberlite field; RKF= Raichur kimberlite field; NKF= Narayanpet kimberlite field; RLF= Ramadugu lamproite field; KLF= Krishna lamproite field; VLF= Vattikod lamproite field. Elchuru (E), Kotappakonda (K), Purimetla (P), Uppalapadu (U) and Errakonda (Ek). **b** Stratigraphic column of the Cuddapah basin (after Nagaraja Rao et al. 1987; Anand et al. 2003) showing the associated igneous rocks and their radiometric ages **c** Garledinne lamproite dyke of this study showing cross-cutting relationship with the Tadpatri shales

0003 lamproite recorded by Joy et al. (2012). The dyke shows pinching and swelling and extends for about 30 m along strike. Based on the age grouping of 1287–1370 Ma for some of the zircons recovered from heavy mineral stream samples in the Banganapalle waste dumps, Joy et al. (2012) infer the emplacement age of these lamproites to be Mesoproterozoic (1.28–1.37 Ga). We have obtained a slightly older whole-rock $^{40}Ar/^{39}Ar$ plateau age of 1433± 8 Ma (2 σ) for a sample collected from the Garledinne lamproite (written comm. Ray Burgess, Manchester).

Sampling and analytical work

Samples of the freshest looking surface material were collected from the Garledinne dyke along its strike. Petrographic studies were carried out by deploying an Olympus BX51 research petrological microscope at the Department of Geology, BHU, Varanasi. Minerals were analysed using a CAMECA-SX100 electron microprobe (EPMA) at Mineral Resources, Technical University of Clausthal, Germany. The analyses were carried out using wavelength-dispersive spectrometry.

An accelerating voltage of 15 kV (for major elements) and 20 kV (for trace elements), a beam current of 50 nA and a beam diameter of 1 μm were used employing TAP, PET and LIF crystals and a PAP online correction program. Several in-house natural and synthetic standards were used for calibration. After repeated analyses it was found that the error on major element concentrations is <1 % whereas the error on trace elements varied between 5 and 10 %.

Whole-rock chemical analysis of five samples, carefully handpicked and free from xenoliths, was carried out at Activation Laboratories, Ancaster, Canada. After multi-acid digestion, ICP-OES (Model: Thermo-JarretAsh ENVIRO II) was used to analyse major elements and a few trace elements (Sc, V, Ba, Sr, Zr, and Y), whereas ICP-MS (Model: Perkin Elmer Sciex ELAN 6000) was used to determine the remaining trace and rare-earth element concentrations. STM1 MRG1, DNC1, W2, and SY3 were used as internal standards and the precision is approximately 5 and 5–10 % for the major oxides and trace elements, respectively, when reported at 100x detection limit. The analytical procedure is detailed by Gale et al. (1997) and available at the Activation Laboratories Ltd website (http://www.actlabs.com). The mineral chemistry data is presented in Tables 1, 2, 3, 4 and 5 and whole-rock geochemical data is provided in Table 6.

Petrography

Petrographic studies by optical microscopy and back-scattered electron imaging (Fig. 2a–f) reveal that the Garledinne lamproite has undergone varying degree of pervasive (deuteric or hydrothermal) silicification and carbonate alteration. However, the overall texture and some relict primary mineralogy are preserved and provide important insights into the original nature of the protolith. The lamproite is porphyritic to weakly porphyritic and contains olivine macrocrysts as well as microphenocrysts (identified by their habit) entirely pseudomorphosed either by carbonate or by silica. The presence of pseudomorphed olivine is further supported by the substantial amounts of Ni, Cr and V (see 'Geochemistry' section below) in these rocks. Highly pleochroic phlogopite is the most abundant pristine phase preserved in these rocks. It is present mostly in a size ranging from 150 to 500 μm as phenocrysts, microphenocrysts and very rarely as irregular poikilitic crystals in the matrix (Fig. 2a, b and c). Phlogopite is orange–yellow with a reddish tinge, which is widely regarded to be a characteristic feature of titanium-rich micas (Mitchell and Bergman 1991). Alteration of phlogopite to chlorite and serpentine is mostly seen at the margins and rare carbonatised laths are also present. The groundmass chromian spinel (up to ~50 μm), apatite and rutile constitute the

Table 1 Representative mineral chemistry composition (oxide wt%) of phlogopite from the Garledinne lamproite dykes. (R) represents rim composition whereas all other data are from cores

Oxide (wt%)	CB-KVS-2	NVC-GDL-1	NVC-GDL-1R	NVC-GDL-1	NVC-GDL-2	NVC-GDL-2	NVC-GDL-2
SiO_2	40.85	41.1	40.27	41.17	40.24	40.52	41.85
TiO_2	7.23	6.37	7.7	6.07	7.77	6.63	5.83
Al_2O_3	9.52	9.98	8.76	9.98	9.44	9.83	10.41
FeO_T	8.51	8.14	10.63	6.12	8.14	7.27	6.84
MnO	0.06	0.02	0.04	0.03	0.04	0.07	0.03
MgO	20.48	22.19	19.35	21.96	20.14	21.08	22.7
CaO	0.02	0.04	0.01	0	0.02	0.01	0.02
Na_2O	0.09	0.09	0.01	0.17	0.09	0.07	0.11
K_2O	9.82	9.02	8.39	9.82	9.87	9.28	8.29
Total	96.58	96.95	95.16	95.32	95.75	94.76	96.08
Cations per 22 oxygen atoms							
Si	5.856	5.826	5.877	5.904	5.819	5.867	5.907
Ti	0.779	0.679	0.845	0.655	0.845	0.722	0.619
Al	1.608	1.667	1.507	1.687	1.609	1.677	1.732
$Fe^{(ii)}$	1.020	0.965	1.297	0.734	0.984	0.880	0.807
Mn	0.007	0.002	0.005	0.004	0.005	0.009	0.004
Mg	4.377	4.689	4.210	4.695	4.342	4.550	4.776
Ca	0.003	0.006	0.002	0.000	0.003	0.002	0.003
Na	0.025	0.025	0.003	0.047	0.025	0.020	0.030
K	1.796	1.631	1.562	1.796	1.821	1.714	1.492
Total	15.47	15.49	15.31	15.52	15.45	15.44	15.37
Mg/Mg+Fe	0.81	0.83	0.76	0.86	0.82	0.84	0.86

Table 2 Mineral chemistry composition (oxide wt%) of phlogopite from the Garledinne lamproite dykes

Oxide (wt%)	NVC-GDL-2	NVC-GDL-1	NVC-GDL-1	NVC-GDL-1	NVC-GDL-1	NVC-GDL-1
SiO_2	41.09	41.95	41.67	42.72	41.38	41.95
TiO_2	6.09	6.13	6.08	6.07	6.04	6.13
Al_2O_3	10.24	10.07	9.91	9.75	9.94	10.07
FeO_T	6.3	6.45	6.69	6.64	6.33	6.45
MnO	0	0	0.03	0.01	0.06	0
MgO	22.23	22.47	22.5	22.06	22.15	22.47
CaO	0.02	0.05	0.04	0.03	0.02	0.05
Na_2O	0.14	0.13	0.15	0.11	0.2	0.13
K_2O	8.85	9.59	9.6	9.57	7.59	9.59
Total	94.96	96.84	96.67	96.96	93.71	96.84
Cations per 22 oxygen atoms						
Si	5.883	5.912	5.896	6.005	5.956	5.912
Ti	0.656	0.650	0.647	0.642	0.654	0.650
Al	1.728	1.672	1.653	1.615	1.686	1.672
$Fe^{(ii)}$	0.754	0.760	0.792	0.781	0.762	0.760
Mn	0.000	0.000	0.004	0.001	0.007	0.000
Mg	4.745	4.721	4.746	4.623	4.753	4.721
Ca	0.003	0.008	0.006	0.005	0.003	0.008
Na	0.039	0.036	0.041	0.030	0.056	0.036
K	1.616	1.724	1.733	1.716	1.394	1.724
Total	15.42	15.48	15.52	15.42	15.27	15.48
Mg/Mg+Fe	0.86	0.86	0.86	0.86	0.86	0.86

Table 3 Representative mineral chemistry composition (oxide wt%) of groundmass spinel (core) from the Garledinne lamproite dykes

Oxide wt%	CB-KVS-1	CB-KVS-1	CB-KVS-1	CB-KVS-1	CB-KVS-2	CB-KVS-1	CB-KVS-1	CB-KVS-1	CB-KVS-2	NVC-GDL-1
TiO_2	3.32	3.25	3.14	3.14	3.41	3.4	3.39	3.01	3.11	3.46
Al_2O_3	2.9	2.9	3.03	2.79	2.6	2.33	2.29	2.67	2.61	2.65
Cr_2O_3	53.48	54.8	57.2	55.81	54.71	51.92	52.23	54.48	54.12	52.61
Fe_2O_3	6.44	7.34	7.12	6.31	5.54	6.49	6.84	5.99	6.48	6.43
FeO	26.37	20.28	16.28	21.31	26.07	30.04	29.89	24.73	23.25	27.33
MnO	0.62	0.79	1.01	0.9	0.65	0.37	0.32	0.58	0.73	0.65
MgO	4.95	8.43	11.22	8.09	5.36	2.59	2.62	5.8	6.61	3.98
CaO	0.29	0.77	0.56	0.15	0.03	0.15	0.42	0.07	0.12	0.49
Total	98.36	98.55	99.56	98.50	98.38	97.29	98.01	97.33	97.03	97.60
Cations per 32 oxygen atoms										
Ti	0.719	0.684	0.642	0.664	0.738	0.761	0.753	0.656	0.675	0.764
Al	0.985	0.957	0.970	0.925	0.881	0.817	0.797	0.911	0.888	0.916
Cr	12.181	12.129	12.290	12.411	12.443	12.209	12.175	12.472	12.354	12.136
V	0.000	0.000	0.000	0.000	0.000	0.000	0.000	0.000	0.000	0.000
$Fe^{(iii)}$	1.395	1.545	1.456	1.336	1.200	1.453	1.521	1.305	1.407	1.420
$Fe^{(ii)}$	6.353	4.748	3.700	5.012	6.271	7.471	7.386	5.988	5.614	6.707
Mn	0.151	0.187	0.232	0.214	0.158	0.093	0.080	0.142	0.179	0.162
Mg	2.126	3.519	4.546	3.392	2.299	1.148	1.154	2.504	2.845	1.741
Ca	0.090	0.231	0.163	0.045	0.009	0.048	0.133	0.022	0.037	0.154
Total	24	24	24	24	24	24	24	24	24	24

Table 4 Representative mineral chemistry composition (oxide wt%) of apatite (core) from the Garledinne lamproite dykes

Oxide wt%	CB-KVS-1	CB-KVS-1	CB-KVS-1	CB-KVS-1	CB-KVS-1	CB-KVS-1	CB-KVS-1	CB-KVS-2
CaO	50.23	50.63	50.80	50.85	50.90	50.13	49.68	50.27
Na_2O	0.07	0.08	0.06	0.04	0.06	0.05	0.05	0.04
SrO	3.26	3.19	3.05	2.95	2.41	2.75	3.44	2.48
FeO	0.26	0.20	0.37	0.32	0.22	0.22	0.14	0.18
MnO	0.04	0.01	0.01	0.01	0.02	0.01	0.01	0.03
MgO	0.18	0.09	0.83	0.17	0.19	0.43	0.09	0.08
La_2O_3	0.47	0.48	0.45	0.55	0.42	0.51	0.44	0.58
Ce_2O_3	1.08	0.89	0.90	1.19	0.95	1.08	1.00	1.31
Pr_2O_3	0.04	0.07	0.03	0.03	0.03	0.07	0.07	0.07
Nd_2O_3	0.38	0.38	0.30	0.43	0.33	0.34	0.35	0.46
Sm_2O_3	0.03	0.01	0.14	0.02	0.13	0.10	0.02	0.08
P_2O_5	42.83	42.43	42.47	43.13	42.62	43.11	42.21	42.17
SiO_2	0.83	0.77	0.66	0.77	1.19	0.65	0.67	1.20
Total	99.23	100.07	100.46	99.47	99.45	98.17	98.95	99.23
Cations per 25 oxygen atoms								
Ca	8.987	9.112	9.071	9.032	9.084	8.959	9.038	9.058
Na	0.023	0.026	0.019	0.013	0.019	0.016	0.016	0.013
Sr	0.316	0.311	0.295	0.284	0.233	0.266	0.339	0.242
Fe	0.036	0.028	0.052	0.044	0.031	0.031	0.020	0.025
Mn	0.006	0.001	0.001	0.001	0.003	0.001	0.001	0.004
Mg	0.045	0.023	0.206	0.042	0.047	0.107	0.023	0.020
La	0.029	0.030	0.028	0.034	0.026	0.031	0.028	0.036
Ce	0.066	0.055	0.055	0.072	0.058	0.066	0.062	0.081
Pr	0.002	0.004	0.002	0.002	0.002	0.004	0.004	0.004
Nd	0.023	0.023	0.018	0.025	0.020	0.020	0.021	0.028
Sm	0.002	0.001	0.008	0.001	0.007	0.006	0.001	0.005
P	6.056	6.034	5.992	6.053	6.011	6.088	6.068	6.004
Si	0.139	0.129	0.110	0.128	0.198	0.108	0.114	0.202
OH	1.000	1.000	1.000	1.000	1.000	1.000	1.000	1.000
Total	16.730	16.777	16.857	16.731	16.739	16.703	16.735	16.722

accessory phases and carbonate (mostly calcite), chlorite, quartz and barite constitute the secondary phases present in varying amounts. Apatite is a common accessory phase and occurs in three modes: (i) inclusions in phenocrysts and microphenocrysts of phlogopite (Fig. 2d); (ii) subhedral prismatic grains or crystal groups in the groundmass (Fig. 2d); and (iii) acicular laths of up to 500 μm in length (Fig. 2f). Occasional oval to sub-rounded xenocrysts of carbonate (Fig. 2c), derived from the carbonate horizons of the Vempalle Formation with shaly intercalations (of the Tadpatri Formation), are also present.

Mineral chemistry

The chemical compositions of phlogopite (Tables 1 and 2) spinel (Table 3), apatite (Table 4) and carbonate, chlorite and rutile (Table 5) in the Garledinne lamproite are briefly summarized here. EPMA studies (Tables 1 and 2) reveal that the phlogopite exhibits a wide compositional range in its TiO_2 (5.83–7.77 wt%), Al_2O_3 (8.76–10.41 wt%) and FeO_T (6.12–10.63 wt%) content. In Mg/(Mg+Fe) and Si (atoms per formula unit) space (Fig. 3a) the samples are compositionally similar to phlogopite from the other Cuddapah and Ramadugu lamproites and are distinct from those of the Krishna lamproites which are more evolved and some of which are biotite. In terms of TiO_2 and Al_2O_3 composition (Fig. 3b), phlogopite in the Garledinne lamproite is similar to that from the: (i) Cuddapah, Krishna and Ramadugu lamproites and (ii) Leucite Hills lamproites (U.S.A), West Kimberley lamproites (Australia), and the Mediterranean lamproites (Fig. 3b). With increasing titanium content, the Garledinne phlogopite displays a moderate decrease in alumina (Fig. 3b) similar to other Indian lamproites, but lacks strong

Table 5 Representative mineral chemistry composition (oxide wt%) of carbonate, chlorite and rutile from the Garledinne lamproite dyke

Carbonate								
Oxide wt%	CB-KVS-1	CB-KVS-1	NVC-GDL-2	NVC-GDL-2 (Xenolith)	NVC-GDL-2 (Xenolith)			
MgO	1.38	0.23	0.09	0.1	0.35			
SiO_2	1.56	1.64	1.11	0.06	0.27			
CaO	49.85	56.96	59.66	53.69	54.22			
MnO	0.64	0.59	0.52	0.52	0.86			
FeO	0.93	1.13	0.53	0.13	0.21			
SrO	0.13	0.05	1.6	1.47	2.14			
Total	55.5	60.89	63.51	56.35	60.05			
Chlorite								
Oxide wt%	CB-KVS-1	CB-KVS-1	CB-KVS-1	CB-KVS-1	CB-KVS-1	CB-KVS-2	CB-KVS-2	NVC-GDL-2
Na_2O	0.02	0.02	0.02	0.01	0.01	0.01	0.03	0.01
MgO	24.12	24.05	25.47	24.02	24.67	25.96	24.52	21.68
Al_2O_3	14.89	14.75	15.54	14.19	15.2	15.44	14.56	15.74
SiO_2	32	31.64	32.28	30.28	31.77	31.8	33.58	37.53
K_2O	0.89	0.99	0.91	0.2	0.71	0.28	2.02	0.02
CaO	0.06	0.04	0.04	0.07	0.05	0.04	0.07	0.23
TiO_2	3.6	5.23	1.27	6.01	3.53	2.34	1.89	0.01
FeO	13.05	12.95	13.26	13.05	13	13.08	12.6	13.27
NiO	0.12	0.15	0.11	0.12	0.17	0.15	0.09	0.01
Total	88.91	89.95	89.08	88.05	89.29	89.25	89.68	88.6
Rutile								
Oxide wt%	CB-KVS-2	CB-KVS-2	CB-KVS-2					
TiO_2	96.45	99.25	98.78					
FeO	1.65	0.29	0.2					
ZrO_2	0.06	0.08	0.37					
Nb_2O_5	2.56	1.19	0.94					
Ta_2O_5	0.02	0.02	0.05					
Total	100.74	100.83	100.34					

Table 6 Bulk-rock geochemistry of the Garledinne lamproite dykes

Oxide (wt%)	NVC/KVS/CB/1	NVC/KVS/CB/2	NVC/GDL/CB	NVC/GDL/A	NVC/GDL
	Co-ordinates: N15°18'27"; E78°00'118"				
SiO_2	44.64	44.69	46.12	47.42	47.71
Al_2O_3	6.35	6.65	6.07	5.98	5.98
$Fe_2O_3^{(T)}$	7.35	7.47	7.55	6.52	6.5
MnO	0.142	0.137	0.12	0.078	0.078
MgO	9.99	10.09	11.4	8.3	8.39
CaO	12.75	12.49	10.6	13.43	13.46
Na_2O	0.03	0.02	0.02	0.04	0.04
K_2O	0.44	0.49	0.79	0.09	0.09
TiO_2	3.504	3.513	3.377	4.016	3.942
P_2O_5	1.23	1.15	1.07	1.62	1.61
LOI	12.3	12.55	11.87	10.19	10.18
Total	98.73	99.25	99	97.69	97.99
Mg #.	77.37	75.94	79.16	76.20	76.45
ppm					
Sc	16	16	15	21	21
V	130	127	124	113	115
Ba	860	881	1423	5512	5645
Sr	1335	1301	1522	1160	1156
Y	17	17	13	44	44
Zr	922	906	881	1915	1940
Cr	660	660	690	390	340
Co	42	42	42	32	28
Ni	430	430	480	250	220
Cu	30	30	20	30	30
Zn	80	80	80	30	<30
Ga	18	18	16	21	18
Rb	12	13	21	3	3
Nb	134	120	129	158	130
Cs	1	1	0.9	<0.5	<0.5
Hf	20	20.1	18.6	36.5	31.6
Ta	8.5	8.6	7.7	10.5	8.7
Pb	27	27	18	9	7
Th	18.4	17.9	15.8	20.2	17.2
U	2.9	3.1	1.9	6.8	5.8
La	272	269	243	334	285
Ce	509	502	455	666	567
Pr	50.3	49.7	44.8	69.7	59.5
Nd	170	168	150	250	215
Sm	18.7	18.2	16.2	32.4	27.6
Eu	4.6	4.5	3.79	7.48	6.44
Gd	9.7	9.4	8.1	18.8	16
Tb	1	1	0.8	2.3	1.9
Dy	4	3.9	3.3	10.5	9
Ho	0.6	0.6	0.5	1.7	1.4
Er	1.3	1.3	1	4	3.4
Tm	0.15	0.16	0.12	0.49	0.42
Yb	0.9	0.9	0.7	2.6	2.3
Lu	0.12	0.12	0.1	0.36	0.31

Mg #=100 Mg / (Mg+Fe)

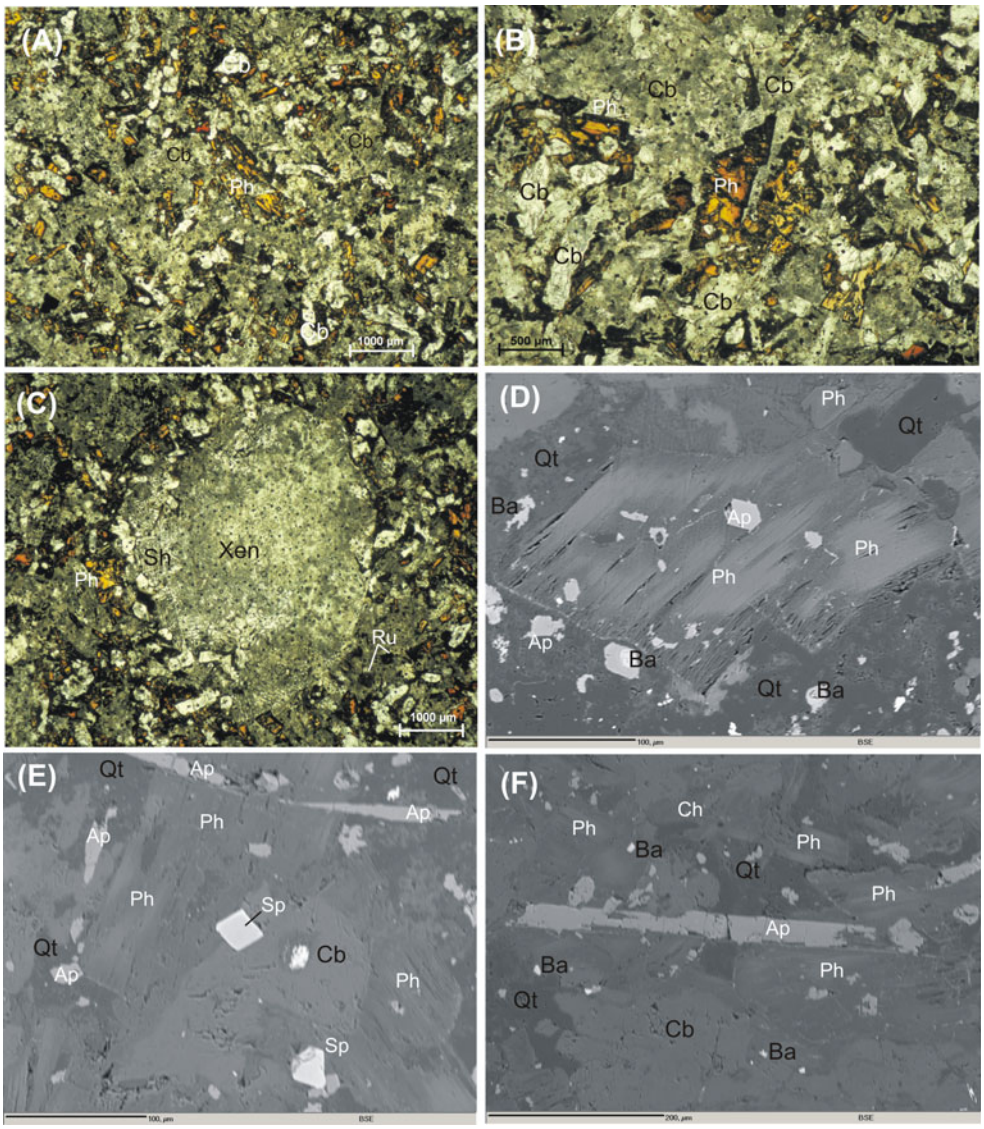

Fig. 2 Photomicrographs and back scattered electron images (BSE) of the Garledinne lamproites **a** Overall texture of the lamproites; Note the alteration due to carbonatization and abundance of phlogopite in the matrix (NVC/GDL/CB; plane light); **b** A higher magnification image showing the variably sized deep-orange laths of phlogopite with reddish margins (NVC/GDL/A; plane light); **c** A large (~2 mm sized) carbonate xenolith with shaly intercalations at its left-hand edge entrained in the lamproite; note the presence of rutile and phlogopite in the groundmass (NVC/GDL; plane light); **d** BSE image showing partially carbonated matrix phlogopite and associated euhedral apatite (NVC/GDl); **e** BSE image showing variably sporadic distribution of spinel in a matrix dominated by carbonate and phlogopite (NVC/KVS/CB-1); and **f** Apatite (up to 200 μm) also occurs in acicular habit in the groundmass ((NVC/KVS/CB-2). Abbreviations: *Cb* carbonate, *Ph* phlogopite, *Ru* rutile, *Sp* spinel, *Ap* apatite, *Xen* carbonate xenolith, *Sh* shaly intercalations, *Ba* barite, *Ch* chlorite, *Qt* quartz

Al depletion characteristic of some lamproites (Mitchell and Bergman 1991).

Spinel from the Garledinne lamproite is chromite and rarely magnesiochromite (Table 3; Fig. 4a). When projected on to the front face of a reduced Fe spinel prism, the Garledinne lamproite spinels do not display a marked titanian magnetite (T2) trend that is similar to the trend displayed by spinel from lamproites and orangeites (Fig. 4b; Mitchell 1995). However, the range in $Fe^{2+}/(Fe^{2+}+Mg)$ at relatively constant high Cr# does appear to be distinctive of lamproites (cf. Barnes and Roeder 2001). Chromian spinel is absent from other Cuddapah lamproites and the wide range of chemical variation displayed by the Garledinne chromian spinel is analogous to that of the chromian spinel from the Ramadugu lamproites (Fig. 4b). However, the Ti content of the Garledinne chromian spinel is markedly lower than that reported from the chromian spinel of Late Cretaceous ultrapotassic rocks from the Damodar valley, eastern India, also shown for comparison in Fig. 4b.

Strontium enrichment (SrO up to 3.44 wt%) is a characteristic feature (Table 4) of apatite from the Garledinne lamproite and in terms of SrO and CaO contents it is indistinguishable from the apatite compositions reported from the Cuddapah, Ramadugu, Damodar valley and West Kimberley lamproites (Fig. 5); however, all of them are quite distinct from apatite of the Krishna lamproites which is much impoverished in SrO (Fig. 5). The abundance of light rare earth elements (viz., La_2O_3 up to 0.58 wt% and Ce_2O_3 up to 1.31 wt%) implies that apatite is the main REE host in the Garledinne lamproite dykes.

Compositions of the carbonate component (including that occurring in carbonate xenoliths), chlorite and rutile are presented in Table 5. The data show little variation. Rutile is characteristically niobian (Nb_2O_5 up to 2.56 wt%) and iron

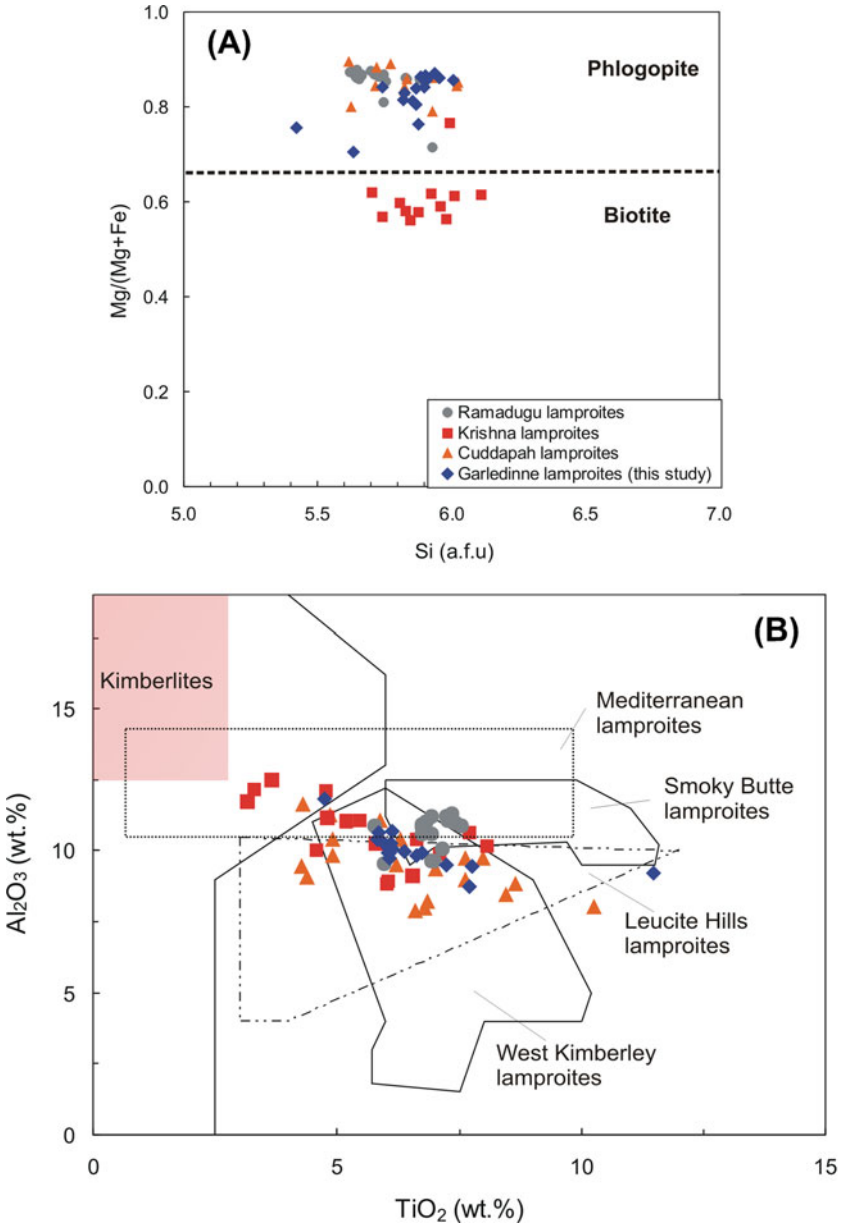

Fig. 3 **a** Si (atoms per formula unit) versus Mg/(Mg+Fe) mica classification diagram (after Reider et al. 1998). Data sources: Krishna lamproites (Paul et al. 2007; Chalapathi Rao et al. 2010); Cuddapah lamproites (Chelima and Zangamarajupalle) (Chalapathi Rao et al. 2004; Chalapathi Rao 2007); Ramadugu lamproites (Chalapathi Rao et al. 2014a). **b** TiO_2 vs Al_2O_3 (wt%) variation plot for groundmass phlogopite. Data symbols and sources are the same as in Fig. 3a. Fields of kimberlites, Leucite Hills, West Kimberley, Smoky Butte and Mediterranean lamproites are taken from Gibson et al. (1995 and the references therein) and Fritschle et al. (2013)

bearing (FeO up to 1.65 wt%) (Table 5). Such niobian rutiles have been reported from the Chelima lamproite (Chalapathi Rao 2011) and also from ultrapotassic rocks from the Damodar Valley, eastern India (see Chalapathi Rao et al. 2014b and references therein).

Whole-rock geochemistry

The whole-rock chemistry of the Garledinne lamproites is presented in Table 6 and is evaluated here in conjunction with such data generated by Joy et al. (2012). The Garledinne lamproites have restricted ranges of SiO_2 (44.64–47.42 wt%), MgO (8.3–11.4 wt%) and Mg# (75–77; Table 6) which are indistinguishable from those of the Cuddapah, Ramadugu and Krishna lamproites (Fig. 6a). Decreasing MgO is accompanied by an increase in SiO_2 implying crystal fractionation. Potassium (K_2O: 0.09–0.44 wt%) contents are low, consistent with the altered nature of some of the phlogopite crystals and the absence of K-feldspar (sanidine), but nevertheless far exceed that of sodium (Na_2O: 0.02–0.04 wt%) identifying the rock as distinctly ultrapotassic (Table 6). In the K_2O/Al_2O_3 versus SiO_2 (wt %) diagram for classifying ultrapotassic rocks (Fig. 6b), the Garledinne lamproites show a marked affinity with those from the Roman province and some samples plot in the field of kamafugites. Their lower K_2O/Al_2O_3 ratio, compared to other

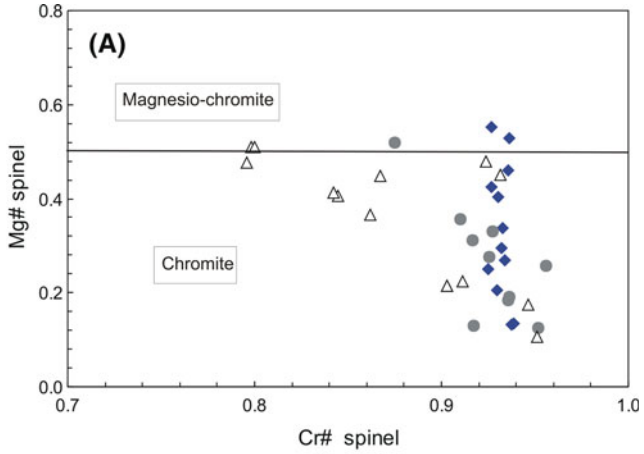

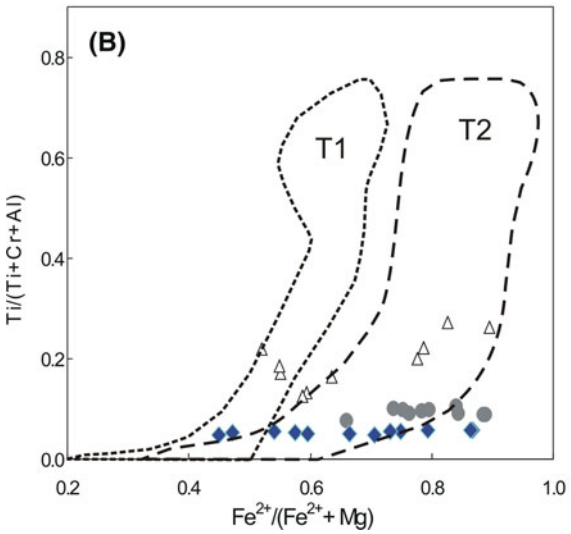

Fig. 4 **a** Mg# [Mg/Mg+Fe^{2+}] versus Cr# [Cr/Cr+Al] (after Pe-Piper et al. 2014) showing the compositional range of the spinel in this study. Open triangles represent spinel composition from 117 Ma ultrapotassic rocks from Damodar valley, eastern India (Mitchell and Fareeduddin 2009; Chalapathi Rao et al. 2014b) shown for comparison. Symbols and sources for the other lamproite spinel data are the same as in Fig. 3a. **b** Compositional variation of spinel from the Garledinne lamproites of this study projected onto the front face of a reduced spinel prism. Compositional fields and trends for spinel from kimberlites (T1) and lamproites (T2) are taken from Mitchell (1995). Data symbols and their source are the same as in Fig. 4a

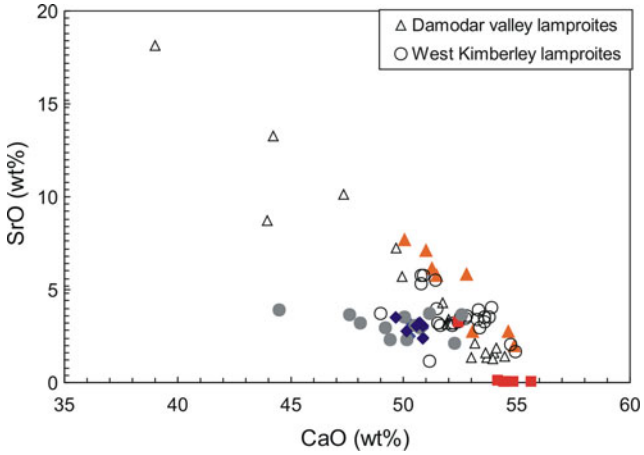

Fig. 5 CaO (wt%) versus SrO (wt%) of apatite from the samples under study. Data symbols and their source are the same as in Fig. 4a. Note the similarity in composition of Garledinne apatite with that from Ramadugu

Cuddapah lamproites (Fig. 6b) is due to the altered nature of their micas (above), but despite their silicification their whole-rock SiO_2 contents are comparable with those of other southern Indian lamproites (Fig. 6b). Generally, Al_2O_3 and TiO_2 constitute the least mobile of the major elements during alteration, and in their bi-variate plot (Fig. 6c) the Garledinne lamproites display strong similarities to the other Cuddapah, EDC and Western Australian lamproites. However, their high TiO_2 contents, a hallmark of lamproites (Foley et al. 1987) and some ultramafic lamprophyres (Tappe et al. 2004), are markedly higher than those from the subduction-related lamproites from Spain and Italy (Fig. 6c). The $Fe_2O_3^{(T)}$ contents of the Garledinne lamproites (6.5–7.47 wt%; Table 6) are lower than those from the Ramadugu (5.93–11.01 wt%; Chalapathi Rao et al. 2014a), Krishna (10.06–27.82 wt%; Paul et al. 2007; Chalapathi Rao et al. 2010) and Cuddapah lamproites (7.08–10.42 wt%; Chalapathi Rao et al. 2004) and reflect the absence of ilmenite and paucity of other iron oxides. Both CaO contents and Loss on Ignition (LOI) of the Garledinne lamproites are >10 wt% (Table 6) and reflect the carbonate and other volatile components. P_2O_5 varies from 1.07 to 1.62 wt% (Table 6) and generally is hosted by apatite.

In the bi-variate plots involving MgO, Al_2O, K_2O, and CaO (Fig. 6d, e and f), the Garledinne lamproites show systematic trends, that might indicate olivine fractionation, and exclude clinopyroxene fractionation as displayed by some of the EDC lamproites. However, the trend shown in Fig. 6d could be a reflection of increasing secondary carbonation, and the trend shown in Fig. 6e very likely indicates increasing secondary carbonate and decreasing K_2O with alteration. Similarly, Al_2O_3 remains fairly constant in Fig. 6f and the increase in CaO probably is related to the secondary carbonate content. Therefore, the trend displayed in this diagram (Fig. 6f) for these Garledinne samples bears no relationship to the illustrated vector, contrary to the apparent trend seen in other Indian lamproites. In order to further evaluate the effects of secondary carbonation and silicification on the whole-rock geochemistry of the Garledinne lamproites, various bi-variate plots involving critical major and trace elements have been additionally deployed. A good correlation is displayed between (i) various major oxides and trace elements [MgO vs Ni (Fig. 7a), MgO vs Cr (Fig. 7b), K_2O vs Rb (Fig. 7c)] and (ii) various LILE (large ion lithophile elements) and HFSE (high field strength elements) including fluid-mobile trace elements such as U and Th [Zr vs Hf (Fig. 7d); Nb vs Ta (Fig. 7e); La vs Zr (Fig. 7f); La vs Ba (Fig. 7g); U vs Th

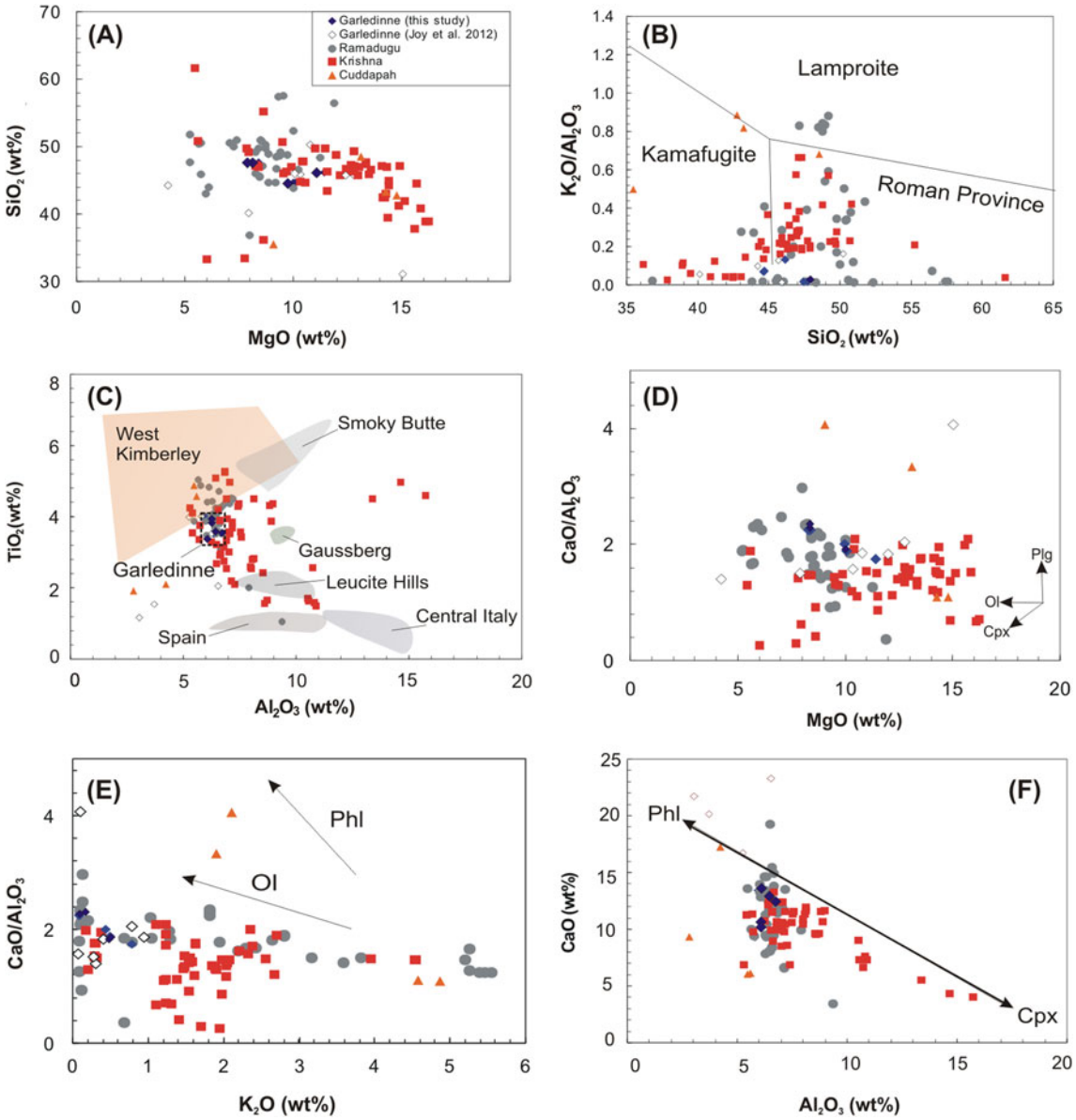

Fig. 6 Major oxide variation (wt%) diagrams of **a** MgO vs SiO_2, **b** SiO_2 vs K_2O/Al_2O_3, **c** Al_2O_3 vs TiO_2 **d** MgO vs CaO/ Al_2O_3, **e** K_2O vs CaO/ Al_2O_3 and **f** Al_2O_3 vs CaO for the Garledinne samples (including those reported by Joy et al. 2012) compared with those from RLF (Chalapathi Rao et al. 2014a); KLF (Paul et al. 2007; Chalapathi Rao et al. 2010); Cuddapah lamproites (Chalapathi Rao et al. 2004; Chalapathi Rao 2007). Various compositional fields shown in (**a**) and (**c**) are from Foley et al. (1987) and Altherr et al. (2004) respectively. The vectors shown in (**e**) and (**f**) are from Kirchenbaur et al. (2012). Data symbols remain the same as in (**a**) for all plots

(Fig. 7h)] demonstrating that despite being subjected to secondary alteration, the bulk-rock composition of the Garledinne lamproites, apart from K_2O and CaO, remained largely unaffected and of petrogenetic significance.

HFSE such as Zr and Nb are considered to be least mobile during low-temperature hydrothermal alteration, and hence are widely used to discriminate between lamproites and kimberlites (e.g. Paton et al. 2009). In such a plot (Fig. 8), the Garledinne samples show stronger affinities to the Ramadugu and Krishna lamproites than to other Cuddapah lamproites. The zirconium contents of the Garledinne lamproites are also elevated implying the possible presence of a zirconium-bearing phase such as zircon, which, however, could not be identified during this study.

Highly fractionated chondrite-normalised REE distribution patterns with a marked enrichment of LREE over HREE (La/Yb up to 347) are a characteristic feature of the Garledinne lamproites (Fig. 9a). Whereas their LREE contents are similar, their HREE display a considerable range suggesting a varying degree of partial melting experienced by their source region.

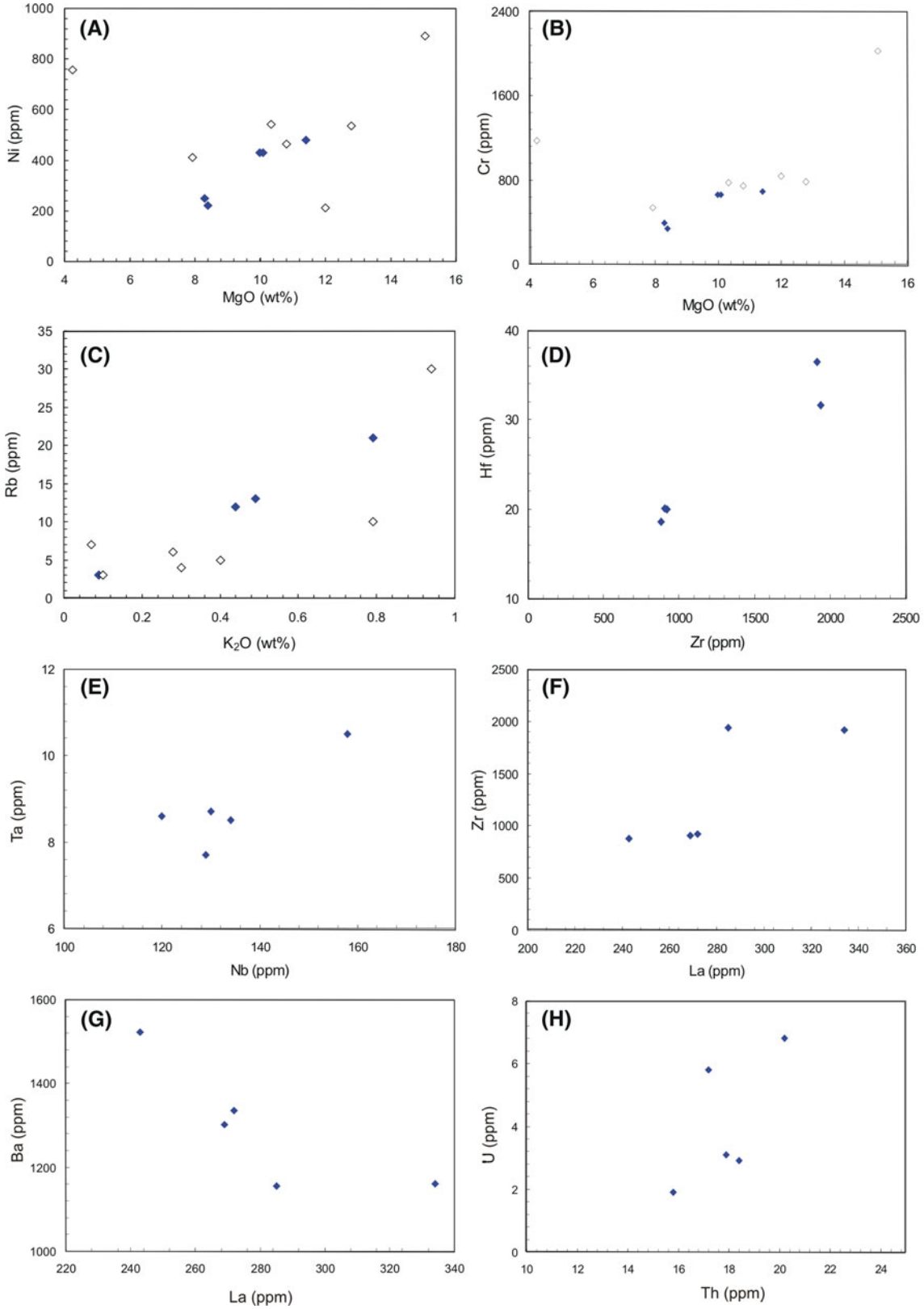

Fig. 7 Bi-variate plots between **a** MgO (wt%) vs Ni (ppm), **b** MgO (wt%) vs Cr(ppm), **c** K_2O (wt%) vs Rb (ppm), **d** Zr vs Hf (ppm), **e** Nb vs Ta (ppm), **f** La vs Zr (ppm), **g** La vs Ba (ppm) and Th vs (U (ppm) for the Garledinne lamproite samples of this study. Data, where available, of Joy et al. (2012) are also shown (*open diamonds*) for comparison. Note the varying degree of good correlation displayed in all plots

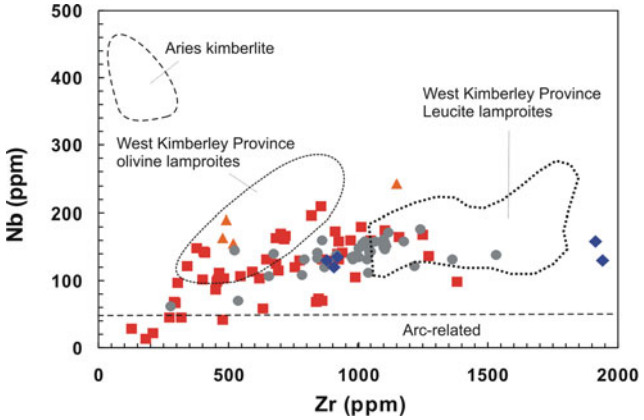

Fig. 8 Zr and Nb (ppm) contents of the Garledinne lamproites compared with those from other lamproites from EDC and Cuddapah basin. The *dotted line* depicts the field of ultrapotassic rocks with very low Nb (<50 ppm) which are considered to be characteristic of subduction-related settings (taken from Sheppard and Taylor 1992) together with the other fields shown for comparison. The data symbols and their sources are the same as in Fig. 6

The REE distribution patterns of the Garledinne lamproites parallel the distribution patterns of lamproites from the Cuddapah, Krishna and Ramadugu (Fig. 9a) suggesting an overall similarity in their genesis.

Primitive-mantle normalised incompatible trace-element patterns of the Garledinne lamproite samples are provided in Fig. 9b. Their incompatible element abundances predominate over those of the primitive mantle with LILE showing a large enrichment in comparison to HFSE. Negative anomalies at Rb, K, Pb and Sr occur in all Garledinne samples whereas such anomalies for U are displayed by only two samples. A number of plausible reasons exist for the anomalies in the multi-element normalized patterns of potassic-ultrapotassic rocks, which attribute them either to: (i) the residual phases in the source; (ii) hydrothermal and/or secondary alteration; or (iii) fractionating phases (see Becker and Le Roex 2006; Coe et al. 2008). Whilst fluid-mobile behaviour of some of these elements (Rb, K, Pb and U) could have partially contributed to their negative anomalies, good correlations amongst many of these elements (Fig. 7) compel us to infer such anomalies to be source-related. The effect of olivine fractionation could also have contributed to the varying depletion (Fig. 9b). An overall similarity, especially for the incompatible trace elements (Sr to Lu) in the multi-element patterns (Fig. 9b) for the Garledinne and other Cuddapah and EDC lamproites as well as ultrapotassic rocks from the Damodar valley, eastern India, additionally suggest similarity in their petrogenetic evolution.

Discussion

The Garledinne lamproite dykes have undergone secondary alteration but their textural aspects (porphyritic to weakly porphyritic), relict minerals and their mineral compositions (Ti-rich phlogopite, chromian spinel, Sr-rich apatite and niobian rutile) and bulk-rock geochemistry (impoverishment of sodium, abundance of LILE, HFSE, high LREE and depleted HREE) are similar to those of other lamproites both in southern Indian and elsewhere (e.g., West Kimberley, Leucite Hills, and Smoky Butte). The Garledinne lamproite strikingly resembles the Chelima and Zangamarajupalle lamproites located elsewhere in the Cuddapah Basin (see Chalapathi Rao et al. 2004; Chalapathi Rao 2007) in having abundant secondary carbonate and a lack of other well-preserved ferro-magnesian phases apart from phlogopite.

There are some conspicuous mineralogical differences between the Cuddapah Basin lamproites (including the Garledinne lamproite) and the EDC lamproites. The Cuddapah Basin lamproites, in general, lack sanidine, clinopyroxene, potassic richterite, and titanite – all of which have been recorded from the EDC lamproites (see Chalapathi Rao et al. 2004, 2010, 2014a). We relate this to either mantle heterogeneity in their source regions or to the difference in the evolution of their magmas. On the other hand minerals such as leucite, priderite, wadeite and perovskite, reported from lamproites worldwide are not found in any of the southern Indian lamproites and they resemble Mediterranean lamproites in this aspect (see Akal 2008). Interestingly, a recent Re-Os isotopic study involving samples from the Krishna lamproite field (KLF; at the NE margin of the Cuddapah Basin) show them to have very radiogenic γOs values (+56 to +355), indicating high Re/Os material – possibly a subducted component – in their source, that are strikingly similar to the compositions of subduction-related lamproites of the Italian peninsula (Chalapathi Rao et al. 2013b). Based on Sr-Nd-Hf-Pb isotopes and major- and trace-element ratios, the involvement of Archaean carbonate-metasomatized subducted komatiite in the source regions of the Krishna lamproites has also been inferred (Chakrabarti et al. 2007). Therefore the mineralogical similarity of the cratonic southern Indian lamproites with that of the Mediterranean lamproites is likely due to similarity in the ancient (Archaean) subduction-related events experienced by the source regions of the former. This aspect merits further evaluation using multi-element isotope systematics involving samples from all the lamproite fields and clusters.

Hydrothermal alteration and the resulting carbonatization and silicification of the Garledinne lamproites can account for their low (<1) perpotassic and peralkaline indices. In fact, extensive secondary alteration appears to be a characteristic feature of all lamproites from the Cuddapah Basin implying a widespread hydrothermal imprint, after lamproite emplacement, across the basin. On the other hand, strong correlations between various major and trace elements and their ratios in the, Garledinne lamproites imply that the geochemical trends (barring those that involve K and Ca) are of primary nature and remained intact despite alteration. Following the modal classification of lamproites (Mitchell and Bergman 1991) the

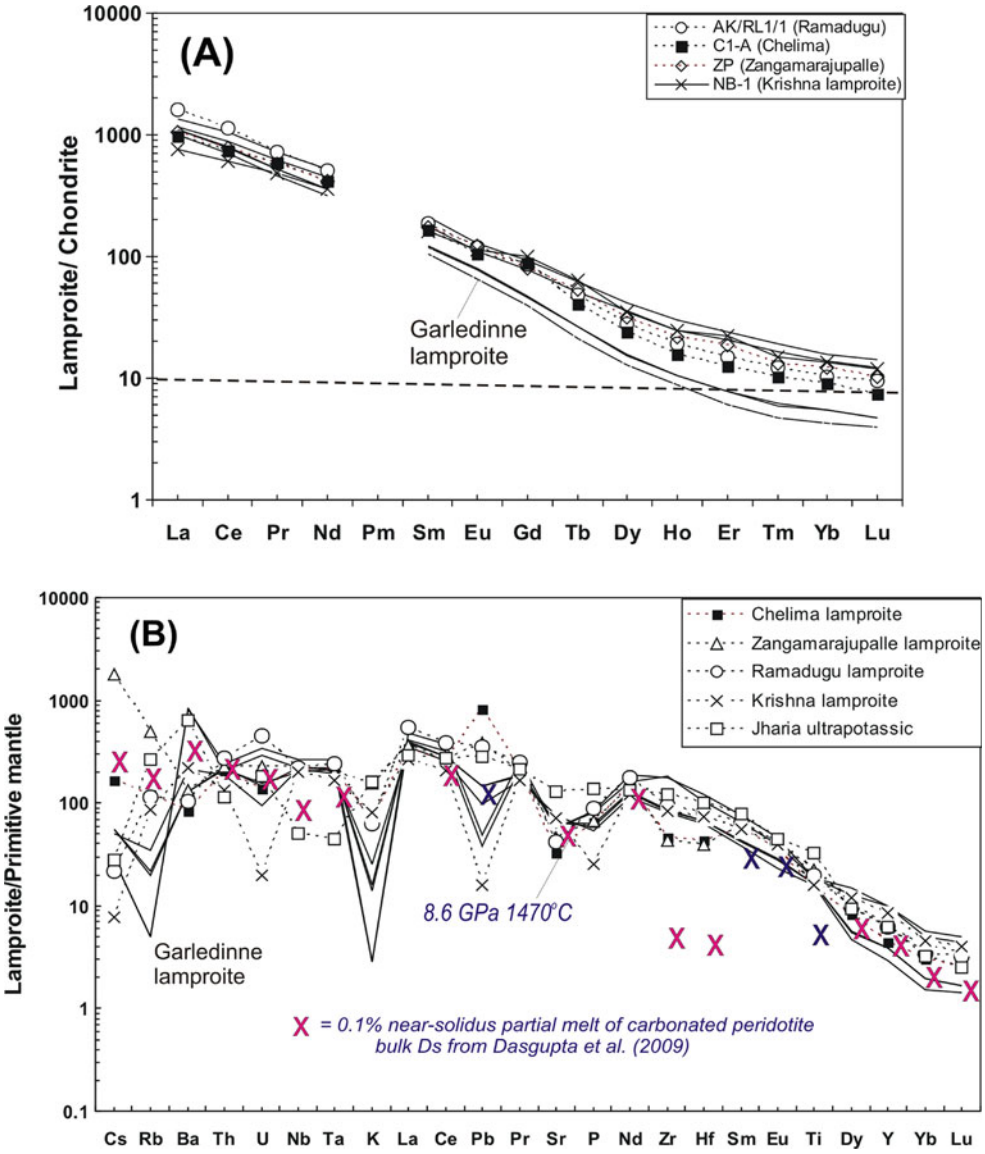

Fig. 9 **a** Chondrite-normalized (after Evenssen et al. 1978) rare earth element distribution patterns (*solid lines*) for lamproites from Garledinne compared with those from representative samples (labelled in the legend) of Ramadugu (Chalapathi Rao et al. 2014a), Chelima and Zangamarajupalle (Chalapathi Rao et al. 2004) and Krishna (Chalapathi Rao et al. 2010) lamproites. Lower (depicted by a dotted line) and variable HREE content is a hall-mark of Garledinne lamproites. **b** Primitive mantle normalized (Palme and O'Neill 2003) multi-element patterns for Garledinne samples of this study compared with those from other lamproites from Cuddapah basin and EDC (data sources are the same as in Fig. 9a, as well as ultrapotassic rocks from Damodar valley, eastern India (data source: Chalapathi Rao et al. 2014b). The crosses represent calculated trace element patterns for near-solidus partial melts of carbonated peridotite at 8.6 GPa (Dasgupta et al. 2009). The model patterns were obtained by using the experimentally determined bulk peridotite/melt partition coefficients and a 0.1 % batch partial melting model adapted from Tappe et al. (2013)

Garledinne dykes correspond to the olivine-phlogopite lamproite variety.

Crustal contamination

With the exception of a solitary carbonate xenolith, no other crustal or mantle xenoliths were observed in the studied Garledinne lamproite samples that contain low silica (SiO_2: 44.64–47.71 wt%), alumina (Al_2O_3: 5.98–6.65 wt%) and particularly low sodium (Na_2O <0.05 wt% Table 6). The Tadpatri Shale of the Cuddapah Supergroup and the granitoids of the EDC, which constitute the basement of the Cuddapah Basin, appear to have had little influence on the composition of the Garledinne lamproites. Assimilation of shale, and felsic minerals such as quartz and feldspar derived from the granitoids, would have resulted in a marked elevation of silica, alumina and sodium that is not the case here. Besides, systematic variation trends displayed between the bulk-rock major and trace elements cannot be explained by assimilation. Furthermore, the abundance of compatible trace elements such as Cr (up to 690 ppm), Ni (up to 480 ppm) and Co (up to 42 ppm), as well as incompatible trace elements such as Sr (up to 1522 ppm), Zr (up to 1940 ppm), Nb (up to 158 ppm) and La (up to 334 ppm) in the Garledinne lamproites is several orders higher in magnitude compared to the continental crust. High Mg # (75–79), highly fractionated REE patterns, low HREE, Y contents and absence of positive Eu and Pb spikes, additionally argue against significant assimilation of crustal material.

The Ce and Nb contents and Ce/Pb and Nb/U ratios of the Garledinne lamproites are: (i) much higher (Fig. 10a and b) than those of average upper- and lower- continental crust material; (ii) close to the supposedly uncontaminated mantle reservoirs such as MORB and OIB; and (iii) strikingly similar to those of other lamproites from the Cuddapah Basin, EDC (especially

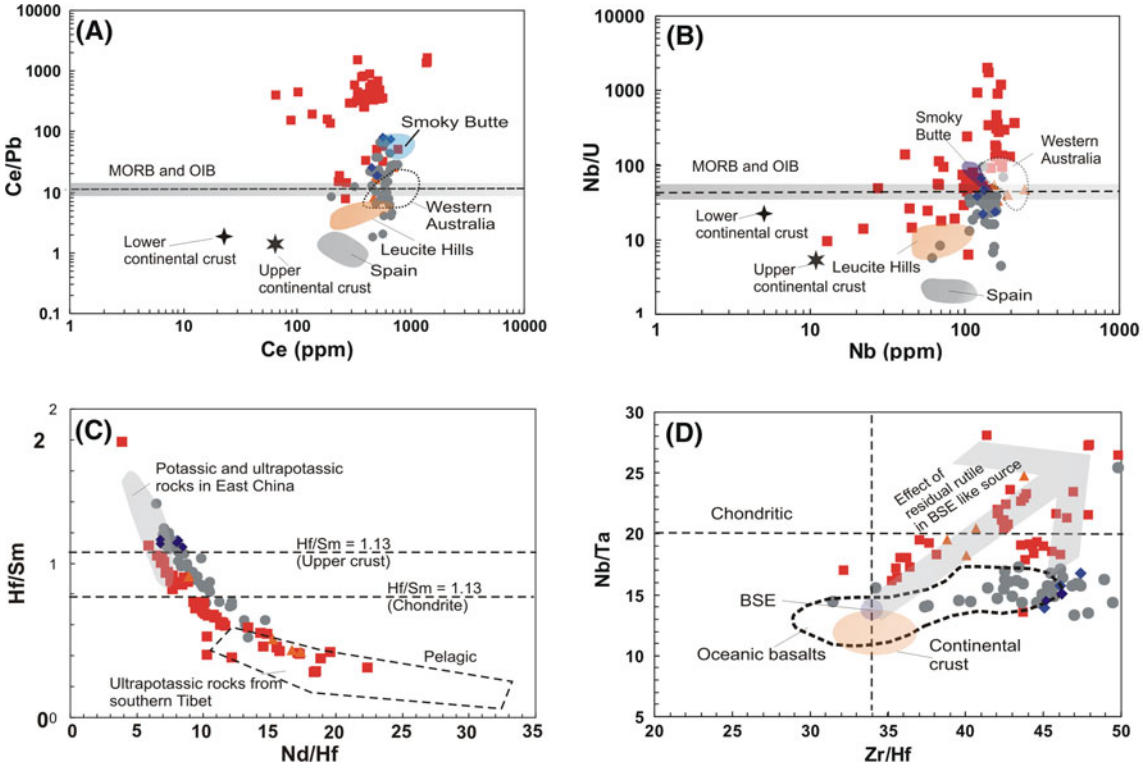

Fig. 10 **a** Ce (ppm) vs Ce/Pb and **b** Nb (ppm) vs Nb/U bi-variate plots for the Garledinne samples compared with those from other lamproites from EDC and Cuddapah basin. The data symbols and their sources are the same as in Fig. 6. The compositional fields of lower continental crust, upper continental crust, MORB and OIB (the range is shown by a *gray* field and median by a *broken line*) are also shown for comparison and are taken from Sun et al. (2014). Various lamproite fields are taken from Davies et al. (2006) and Yilmaz (2010). **c** Nd/Hf vs Hf/Sm plot (after Wang et al. 2014) for the Garledinne lamproites compared with those from other lamproites from EDC and Cuddapah basin. The data symbols and their sources are the same as in Fig. 6. The field of continental subduction-related potassic and ultrapotassic rocks from East China and pelagic material enriched source rocks from southern Tibet are also shown for comparison (Wang et al. 2014). **d** Zr/Hf vs Nb/Ta (after Tappe et al. 2008) of the Garledinne lamproites compared with other EDC and Cuddapah basin lamproites. Data symbols and their sources are the same as in Fig. 6. *Arrow* indicates the trend of a melt formed in the presence of residual rutile in Bulk Silicate Earth-like (BSE) material. Note that Garledinne lamproites exclude crustal contamination and are distinct in their composition to the data of KLF and other Cuddapah lamproites but are strikingly similar to that of RLF

Ramadugu), West Kimberley and Smoky Butte. The Hf/Sm ratios of the Garledinne lamproites slightly overlap with the field of subducted continental crust-derived ultrapotassic rocks from East China but are clearly higher compared to the pelagic material enriched mantle source regions of ultrapotassic rocks from southern Tibet (Fig. 10c). This again excludes significant assimilation of upper crustal and pelagic material either by contamination or by subduction. This inference is also supported by the lack of Nb-Ta-Ti depletions in the primitive mantle normalized multi-element diagrams (Fig. 9 above) and is consistent with the findings from several previous studies on lamproites which revealed that crustal contamination has limited influence on their extremely high incompatible trace element enrichments (e.g. Nelson 1992; Murphy et al. 2002; Davies et al. 2006; Mirnejad and Bell 2006; Chakrabarti et al. 2007).

Mantle source regions

Mantle-derived xenoliths or xenocrysts were not found in the Garledinne lamproites in this study. However, Joy et al. (2012) report a small population of garnets from crushing ~1000 kg of Garledinne lamproite material. Compositionally, these garnets belong to the fertile lherzolitic variety in contrast to the low-temperature depleted harzburgitic variety recorded from the kimberlites of WKF, towards the western margin of the Cuddapah Basin (Sastry et al. 2005). Geochemical characteristics such as high Mg#, abundance of compatible elements (Ni, Cr and Co), and low HREE contents imply a refractory mantle source that had experienced previous melt extraction (e.g. Mitchell and Bergman 1991; Beard et al. 2000; Mirnejad and Bell 2006) in the genesis of the Garledinne lamproites. Extensive extrusive and intrusive mafic magmatic activity (ca. 1.9 Ga) recorded as dykes, sills and volcanic rocks in the Vempalle and Tadpatri Formations of the Cuddapah Supergroup provide evidence for such previous melt extraction (Anand et al. 2003; French et al. 2007). However, the high concentration of incompatible trace elements, e.g., LILE and HFSE (above), highlights the subsequent enrichment of the mantle source that needs to be confirmed by isotopic evidence. Thus, a previously depleted as well as

subsequently enriched mantle source, similar to that found in garnet peridotite nodules (Beard et al. 2007; Gibson et al. 2008) and commonly assumed as the source region of lamproites and kimberlites (e.g. Mitchell and Bergman 1991; Tainton and McKenzie 1994; Becker and Le Roex 2006), is also inferred for the Garledinne lamproites. The presence of xenocrystic garnet (Joy et al. 2012) and high La/Yb and low HREE contents also imply generation of the Garledinne lamproite magma by small degrees of partial melting from an enriched (metasomatised) mantle source within the garnet stability field.

The exact source of the melts and fluids responsible for an enriched (metasomatised) mantle source of potassic–ultrapotassic rocks remains unclear and a variety of models currently exist: (i) subducted lithosphere (e.g., Ersoy et al. 2014; Garza et al. 2013); (ii) convective (asthenospheric) mantle (e.g., McKenzie 1989); (iii) deep-mantle plumes (e.g., Torsvik et al. 2010); and (iv) cratonic sub-continental lithospheric mantle (e.g., McKenzie 1989; Foley 1992; Tappe et al. 2008). The composition of the melts involved in mantle metasomatism can also vary from carbonate and alkali-rich silicate melts to H_2O- and CO_2-rich fluids (e.g., Coltorti et al. 1999; Ionov et al. 2002). The primitive mantle normalized multi-element patterns (Fig. 9b) of the Garledinne lamproites exclude subduction-related signals and their Nb/Pb, and Ce/Pb contents are too high to be products of melts/fluids derived from subducted pelagic sediments (Fig. 10). Negative anomalies at K and Rb in multi-element plots (Fig. 9b) imply the presence of amphibole or phlogopite in the source (see Sato et al. 1997), although alteration has played an important role in leaching of these mobile elements and thereby enlarging the magnitude of these anomalies. Residual clinopyroxene (Tappe et al. 2004) or a source that had previously undergone depletion in Sr due to melt extraction (Mitchell 1995) can account for the depletions in Sr for the Garledinne lamproites (Fig. 9b). Likewise, the slight negative anomalies for P in some of the Garledinne samples suggest the presence of a phosphate in the residue (Mitchell and Edgar 2002). Available experimental evidence also favours phlogopite, potassic richterite, diopside and apatite to be some of the essential phases in lamproite source regions, very likely occurring as metasomatic veins within a lherzolitic or harzburgitic source (e.g., Edgar and Vukadinovic 1992; Foley 1992; Konzett et al. 1997).

The Garledinne lamproites have super-chondritic Zr/Hf (43–46) as well as sub-chondritic Nb/Ta (15–18) (Fig. 10d). An enriched mantle source, with the involvement of an asthenospheric component, is attributed to the super-chondritic Zr/Hf whereas a depleted sub-continental lithosphere is held responsible for sub-chondritic Nb/Ta (see Weyer et al. 2003). The Garledinne lamproites are thus inferred to have been derived from mantle sources that experienced depletion and subsequent enrichment. Zr/Hf and Nb/Ta contents of the Garledinne lamproites (Fig. 10d) are: (i) indistinguishable from those of the Ramadugu lamproites; (ii) markedly dissimilar to those of the other Cuddapah Basin lamproites and a majority of the Krishna lamproites; (iii) lack the effect of residual rutile in the BSE-like source; (iv) exclude signatures of continental crust; and (v) suggest involvement of an asthenospheric (oceanic basalt) component. The lack of Ti depletion in the primitive mantle normalized multi-element plot (Fig. 9b) additionally provides support for the absence of titanite in the residue. Recently, Tappe et al. (2013) calculated trace-element patterns for partial melting of a carbonated peridotite source between 6 and 10 GPa utilizing a fixed 0.1 % batch partial melting model (McKenzie 1985; Gudfinnsson and Presnall 2005) and the source trace-element contents set at primitive mantle values (Palme and O'Neill 2003). The 'bulk' peridotite/melt partition coefficients, reported by Dasgupta et al. (2009), were used for this purpose. The calculated trace-element compositions remarkably match those from the Lac de Gras kimberlites in Canada whose derivation was inferred to be from low-degree partial melting of carbonated peridotite under convective mantle conditions (Tappe et al. 2013). The melting model of Tappe et al. (2013), when adapted for the Garledinne lamproite (Fig. 9b), displays a very good fit for many of the incompatible trace elements suggesting the involvement of carbonated peridotite in their petrogenesis. A similarly good fit has also been observed in the case of other EDC and Cuddapah Basin lamproites and ultrapotassic rocks from Damodar valley (Fig. 9b).

Genesis

The ultimate site where the lamproite source regions have undergone partial melting remains controversial and ranges from the SCLM (e.g., Mitchell 2006; Davies et al. 2006; Avanzinelli et al. 2009) to the transition zone (e.g., Murphy et al. 2002). The poorly defined correlation of La/Yb with La (not shown) implies that partial melting together with fractional crystallization played an important role in the compositional variation of the Garledinne lamproites. Petrography as well as whole rock major-element chemistry have indeed demonstrated (above) olivine fractionation in the Garledinne lamproite dykes. Relatively lower Nb/Y with increasing SiO_2 (wt%) contents (Fig. 11a) suggest that the Garledinne lamproites (together with other lamproites from the Cuddapah Basin and EDC) have been products of much greater degrees of partial melting than the kimberlites from the WKF and NKF. This is likely due to the location of the EDC and Cuddapah Basin lamproites at the margin of the craton where the lithosphere is relatively thin compared to its 'core' (e.g. Priestly and McKenzie 2006; Chalapathi Rao et al. 2010). The Garledinne lamproites have $(La/Sm)_N$ and $(Ho/Lu)_N$ contents indistinguishable from those in the other Cuddapah lamproites and kimberlites from WKF and NKF (not shown) implying

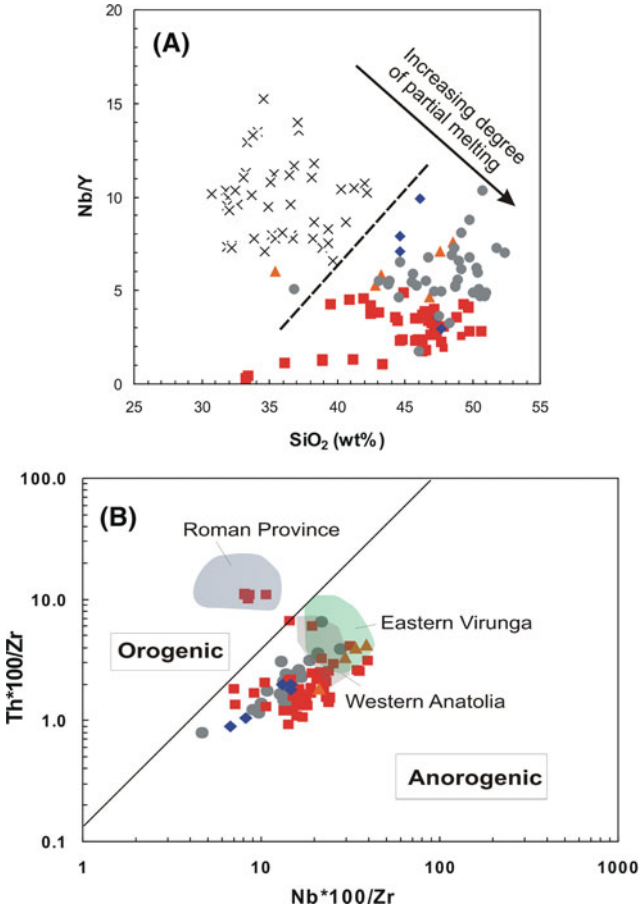

Fig. 11 **a** Nb/Y vs SiO_2 (wt%) diagram (Beard et al. 1998) illustrating the degree of partial melting in the Garledinne lamproites. The data (x) of EDC kimberlites (WKF and NKF) is also shown for comparison and is from Chalapathi Rao et al. (2004) and Chalapathi Rao and Srivastava (2009). Rest of the data symbols and their sources are the same as in Fig. 6b Nb * 100/Zr vs Th * 100/Zr (after Yilmaz 2010) of the Garledinne lamproites depicting their anorogenic geochemical character. Data symbols and their sources are the same as in Fig. 6. Other fields are taken from Yilmaz (2010) and Kullerud et al. (2011)

the involvement of a similar mantle source in their genesis. The involvement of an asthenospheric (MORB and OIB) component in the genesis of the Garledinne lamproites and other lamproites from the Cuddapah Basin and EDC is apparent from their Nb/U, Ce/Pb, Zr/Hf, and Nb/Ta ratios (Figs. 10a–d). Thus, we infer the involvement of multiple reservoirs, viz., SCLM and asthenospheric sources, in the genesis of the Garledinne lamproites. Recent studies of potassic–ultrapotassic rocks have also invoked multiple reservoirs in their genesis (Le Roex et al. 2003; Tappe et al. 2011). The Th/Nb ratio, normalized to Zr (to eliminate the effects of fractional crystallization) can constitute a sensitive discriminator between orogenic and anorogenic tectonic settings of ultrapotassic rocks, with the former being characterized by a higher Th/Nb (see Kullerud et al. 2011). In such a plot (Fig. 11b) the Garledinne lamproites, along with the other lamproites from the Cuddapah Basin and a great majority of EDC are strikingly confined to the anorogenic lamproite field and are similar to the well-known extension-related ultrapotassic lavas of the eastern Virunga and western Anatolia volcanic fields in this aspect.

Diamond potential

Experimental studies show that only olivine lamproites, which originate from depths of at least 150–160 km, can contain diamond whereas high-silica lamproites can be generated from mica harzburgites at fairly low pressures of less than 3 GPa and are essentially non-diamondiferous (Foley 1993). A recent synthesis of global lamproites and their diamond prospectivity lends support to these experimental findings (Birkett 2008). The olivine lamproitic nature of the Garledinne lamproites assumes significance in this context. Even though the Garledinne lamproites are inferred to be sources for the diamonds in the nearby Banganapalle conglomerates, no diamond has actually been recovered in their processing (Joy et al. 2012). However, Coulson (1933) recorded that several sills (their locations and mafic/ultramafic nature were not published) that intruded the lower Cuddapah Supergroup were diamondiferous. Therefore, the diamondiferous nature of the Garledinne (and hitherto unknown) lamproite dykes and sills in the Lower Cuddapah formations remains an open question.

Geodynamic implications

The eruption ages of the lamproites and kimberlites constitute time capsules in a geodynamic framework and are of tectonomagmatic significance (e.g., Jelsma et al. 2009; Foley et al. 2012). Available radiometric ages of the Cuddapah Basin and EDC lamproites show them to be of Mesoproterozoic age with a great majority emplaced between 1.25 and 1.45 Ga (Chalapathi Rao et al. 1999; Kumar et al. 2001; Osborne et al. 2011). These ages are strikingly similar to: (i) the emplacement age (1326±73 Ma) of the Racherla alkali syenite within the Cuddapah Basin (Fig. 1a for location; Chalapathi Rao et al. 2012); (ii) the spectrum of alkaline and sub-alkaline syenite complexes and lamprophyres (1250–1350 Ma) emplaced elsewhere within the Eastern Ghats Mobile Belt, towards the eastern margin of the Cuddapah Basin (Fig. 1a for location; Upadhyay et al. 2006; Kumar et al. 2007); (iii) the whole rock depleted-mantle (T_{DM}) Nd model ages (1.38–1.47 Ma) of the ≥620 Ma Tokapal kimberlite system, Bastar Craton, central India (Lehmann et al. 2007); (iv) the perovskite depleted-mantle (T_{DM}) Nd model ages (1.3–1.5 Ga; Chalapathi Rao et al. 2013a) of the 1.1 Ga NKF and WKF kimberlites, EDC, southern India; and (v) depleted-mantle T_{DM} Nd model ages (1.4–1.5 Ga) of the diamondiferous Majhgawan diatreme of the Bundelkhand Craton, northern India (Lehmann et al. 2006), thereby implying involvement

of regional geotectonic controls, across these cratons and mobile belts, in all kimberlite and lamproite generations.

Available depleted mantle (T_{DM}) Nd model ages (which are minimum ages) indicate that the source regions of the Cuddapah and EDC lamproites were enriched due to a regional metasomatic event at ~2 Ga (Chalapathi Rao et al. 1998, 2004; Chakrabarti et al. 2007). The source regions of alkaline and sub-alkaline syenites and lamprophyres located towards the eastern margin of the Cuddapah Basin, in the Eastern Ghats Mobile belt, also had been affected by this regional metasomatic event (Upadhyay et al. 2006; Kumar et al. 2007) together with the tholeiitic intrusives in the Napier Complex, Enderby Land, Antarctica (Chatterjee and Bhattacharjee 1998), thereby implying that this regional metasomatic event was widespread across the Proterozoic eastern Gondwana. In fact, the long-lived (~2.6 Ga) nature of this regional enrichment event has been demonstrated recently by depleted mantle (T_{DM}) Nd model ages for apatite from the Racherla alkali syenite from within the Cuddapah Basin (Chalapathi Rao et al. 2012). It is very likely that the source region of the Garledinne lamproite has also undergone this regional metasomatic enrichment, and this needs to be confirmed by isotopic studies.

Interestingly, the emplacement ages (1.25–1.45 Ga) of the majority of the lamproites from the Cuddapah Basin and the EDC, and the depleted mantle (T_{DM}) Nd model ages of the kimberlites from the EDC, Bastar and Bundelkhand cratons of India (above), coincide with the break-up of the Paleo-Mesoproterozoic supercontinent of Columbia (Rogers and Santosh 2009; Meert 2012). We consider this coincidence to be of geodynamic significance since the long-term extensional events associated with the break-up of Columbia could have constituted the regional tectonic control capable of triggering not only lamproite eruptions at 1.25–1.45 Ga, but also the enrichment of source regions of kimberlites located at some distance across the various cratons. The geochemical similarity of the Garledinne lamproites to the well-known extension-related ultrapotassic lavas of eastern Virunga and western Anatolia (Fig. 11b) assumes significance in this respect. In fact, a small amount of lithospheric extension, without the need for a mantle plume, has been invoked in the genesis of the kimberlites and lamproites from the EDC and the Cuddapah Basin (Chalapathi Rao et al. 2004, 2010, 2014a), as well as the alkaline rocks occurring within and towards the east of the Cuddapah Basin in the Eastern Ghats Mobile belt (Upadhyay et al. 2006; Chalapathi Rao et al. 2012).

Conclusions

The Garledinne lamproites were subjected to varying degrees of pervasive alteration and are characterized by widespread carbonatization and silicification. They have a porphyritic to weakly porphyritic texture comprising pseudomorphs after olivine, Ti-rich phlogopite microphenocrysts, chromian spinel, Sr-rich apatite and niobian rutile. The Garledinne (and other Cuddapah Basin) lamproites are mineralogically distinct from the Eastern Dharwar Craton lamproites in their lack of sanidine, clinopyroxene, potassic richterite, and titanite. Deuteric alteration and crustal contamination have had limited effect on the whole-rock geochemistry of the Garledinne lamproites and olivine fractionation played a dominant role in their evolution. The Garledinne lamproites probably formed as small-degree partial melts derived from a refractory peridotitic mantle source that was previously enriched by carbonate-rich fluids/melts within the garnet stability field. Both the sub-continental lithospheric mantle and asthenosphere are inferred in the genesis of the Garledinne lamproite dykes. The emplacement of the Garledinne lamproites probably was related to extensional events during the break-up of the Columbia supercontinent.

Acknowledgments It's a great pleasure to contribute to this special issue being brought out in honor of the late Professor Rex Prider whose pioneering studies on lamproites are indeed remarkable. In-depth reviews provided by Felix Kaminsky (Vancouver) and Peter Downes (Perth) as well as editorial suggestions by Johann Raith (Leoben) are thankfully acknowledged. Financial assistance from CSIR (At, AK and NC), UGC (SS) and DST (PN) are thankfully acknowledged. NVCR thanks the Head, Dept. of Geology, BHU and AvH Foundation, Germany, for support.

References

Akal C (2008) K-richterite-olivine-phlogopite-diopside-sanidine lamproite from the Afyon volcanic province, Turkey. Geol Mag 145:570–585

Altherr R, Meyer HP, Holl A, Volker F, Alibert C, McCulloch MT, Majer V (2004) Geochemical and Sr-Nd-Pb isotopic characteristics of Late Cenozoic leucite lamproites from the East European Alpine belt. Contrib Mineral Petrol 147:58–73

Anand M, Gibson SA, Subbarao KV, Kelley SP, Dickin AP (2003) Early Proterozoic melt generation processes beneath the intracratonic Cuddapah Basin, southern India. J Petrol 44:2139–2171

Avanzinelli R, Lustrino M, Mattei M, Melluso L, Conticelli S (2009) Potassic and ultrapotassic magmatism in the circum-Tyrrhenian region: significance of carbonated pelitic vs. Pelitic sediment recycling at destructive plate margins. Lithos 113:213–227

Barnes SJ, Roeder PL (2001) The range of spinel compositions in terrestrial mafic and ultramafic rocks. J Petrol 42:2279–2302

Basu A, Bickford ME (2013) Contributions of zircon U-Pb geochronology to understanding the volcanic and sedimentary history of some Purāna basins, India. J Asian Earth Sci 91:252–262

Beard AD, Downes H, Hegner E, Sablukov SM, Vetrin VR, Balogh K (1998) Mineralogy and geochemistry of Devonian ultramafic minor intrusions of the southern Kola peninsula, Russia: implications for the petrogenesis of kimberlites and melilitites. Contrib Mineral Petrol 130:288–303

Beard AD, Downes H, Hegner E, Sablukov SM (2000) Geochemistry and mineralogy of kimberlites from the Argkhangelsk Region, NW Russia: evidence for transitional kimberlite magma types. Lithos 51: 47–73

Beard AD, Hownes H, Mason PRD, Vetrin VR (2007) Depletion and enrichment processes in the lithospheric mantle beneath the Kola peninsula (Russia): evidence from spinel lherzolite and wehrilite xenoliths. Lithos 94:1–24

Becker M, Le Roex AP (2006) Geochemistry of south African on- and off-craton group I and II kimberlites: petrogenesis and source region evaluation. J Petrol 47:673–703

Bergman SC (1987) Lamproites and other K-rich igneous rocks: review of their occurrence, mineralogy and geochemistry. Geol Soc Lond Spec Publ 30:103–190

Bhattacharji S, Singh RN (1984) Thermomechanical structure of the southern part of the Indian shield and its relevance to Precambrian basin evolution. Tectonophysics 105:103–120

Bickford ME, Saha D, Schieber S, Kamenov G, Russell A, Basu A (2013) New U-Pb ages of zircons in the Owk Shale (Kurnool Group) with reflections on Proterozoic procellanites in India. J Geol Soc India 82:207–217

Birkett TC (2008) First-row transition elements, Y and Ga in kimberlite and lamproite: applications to diamond prospectivity and petrogenesis. Can Mineral 46:1269–1282

Carlier G, Lorand JP (2003) Petrogenesis of a zirconolite-bearing Mediterranean-type lamproite from the Peruvian Altiplano (Andean Cordillera). Lithos 104:15–35

Chakrabarti R, Basu AR, Paul DK (2007) Nd-Hf-Sr-Pb isotopes and trace element geochemistry of Proterozoic lamproites from southern India: subducted komatiite in the source. Chem Geol 236:291–302

Chalapathi Rao NV (2005) A petrological and geochemical reappraisal of the mesoproterozoic diamondiferous majhgawan pipe of central India: evidence for transitional kimberlite- orangeite (Group- II kimberlite) - lamproite rock type. Mineral Petrol 84:69–106

Chalapathi Rao NV (2007) Chelima dykes, Cuddapah basin, southern India: a review of the age, petrology, geochemistry and petrogenesis of World's oldest lamproites. J Geol Soc India 69:523–538

Chalapathi Rao NV (2011) Sr-rich apatite and Nb-rutile from the Chelima lamproite dykes, Cuddapah basin, southern India and their petrological significance. Curr Sci 100:1207–1210

Chalapathi Rao NV, Srivastava RK (2009) Petrology and geochemistry of diamondiferous Mesoproterozoic kimberlites from Wajrakarur kimberlite field, Eastern Dharwar Craton, Southern India: genesis and constraints on mantle source regions. Contrib Mineral Petrol 157: 245–265

Chalapathi Rao NV, Miller JA, Pyle DM, Madhavan V (1996) New Proterozoic K-Ar ages for some kimberlites and lamproites from the Cuddapah Basin and Dharwar craton, southern India. Precambrian Res 79:363–369

Chalapathi Rao NV, Gibson SA, Pyle DM, Dickin AP (1998) Contrasting isotopic mantle sources for Proterozoic lamproites and kimberlites from the Cuddapah Basin and Eastern Dharwar craton: Implication for Proterozoic mantle heterogeneity beneath southern India. J Geol Soc India 52:683–694

Chalapathi Rao NV, Miller JA, Gibson SA, Pyle DM, Madhavan V (1999) Precise $^{40}Ar/^{39}Ar$ dating of Kotakonda kimberlite and Chelima lamproite, India: implication to the timing of mafic dyke swarm activity in the Eastern Dhawar craton. J Geol Soc India 53: 425–432

Chalapathi Rao NV, Gibson SA, Pyle DM, Dickin AP (2004) Petrogenesis of Proterozoic lamproites and kimberlites from the Cuddapah basin and Dharwar cratons, southern India. J Petrol 45: 907–948

Chalapathi Rao NV, Kamde G, Kale HG, Dongre A (2010) Mesoproterozoic lamproites from the Krishna Valley, Eastern Dharwar craton, southern India: Petrogenesis and diamond prospectivity. Precambrian Res 177:103–130

Chalapathi Rao NV, Wu FY, Srinivas M (2012) Mesoproterozoic emplacement and enriched mantle derivation of the Racherla alkali syenite, Palaeo-Mesoproterozoic Cuddapah basin, southern India: Insights from *in situ* Sr-Nd isotopic analysis on apatite. Geol Soc Lond Spec Publ 365:185–195

Chalapathi Rao NV, Wu FY, Mitchell RH, Li Q, Lehmann B (2013a) Mesoproterozoic U–Pb ages, trace element and Sr–Nd isotopic composition of perovskite from kimberlites of the Eastern Dharwar craton, southern India: distinct mantle sources and a widespread 1.1 Ga tectonomagmatic event. Chem Geol 353:48–64

Chalapathi Rao NV, Creaser RA, Lehmann B (2013b) Re-Os isotope study of Indian kimberlites and lamproites: implications for their mantle source regions and cratonic evolution. Chem Geol 353:36–47

Chalapathi Rao NV, Kumar A, Sahoo S, Dongre A, Talukdar D (2014a) Petrology and petrogenesis of Mesoproterozoic lamproites from the Ramadugu field, NW margin of the Cuddapah basin, eastern Dharwar craton, southern India. Lithos 196–197:150–168

Chalapathi Rao NV, Srivastava RK, Sinha AK, Ravikant V (2014b) Petrogenesis of Kerguelen-plume linked ultrapotassic intrusives from the Gondwana sedimentary basins, Damodar valley, eastern India. Earth Sci Rev 136:96–120

Chatterjee N, Bhattacharjee S (1998) Formation of tholeiitic intrusives in and around Cuddapah basin, south India and their Gondwana counterparts in East Antarctica and compositional variation in their mantle sources. Neues Jahrb Miner Abh 174:79–102

Chaudhuri AK, Saha D, Deb GK, Deb SP, Mukherjee MK, Ghosh G (2002) The Purana basins of southern cratonic province of India- a case for Mesoproterozoic fossil rifts. Gondwana Res 5:23–33

Chetty TRK (2011) Tectonics of Proterozoic Cuddapah basin, Southern India: a conceptual model. J Geol Soc India 78:446–456

Coban H, Flower MFJ (2006) Mineral phase compositions in silica-undersaturated 'leucite' lamproites from the Bucak area, Isparta, SW Turkey. Lithos 389:275–299

Coe N, Le Roex A, Gurney JJ, Pearson GD, Nowell G (2008) Petrogenesis of Swartruggens and Star Group II kimberlite dyke swarms, South Africa: constraints from whole rock geochemistry. Contrib Mineral Petrol 156:627–652

Collins AS, Patranabis-Deb S, Alexander E, Bertram CN, Falster GM, Gore RJ, Mackintosh J, Dhang PC, Saha D, Payne JL, Jourdan F, Back'e G, Halverson GP, Wade BP (2014) Detrital mineral age, radiogenic isotopic stratigraphy and tectonic significance of the Cuddapah basin. India Gondwana Res. doi:10.1016/j.gr.2014.10.013

Coltorti M, Bonadiman C, Hinton RW, Siena F, Upton BGJ (1999) Carbonatite metasomatism of the oceanic upper mantle: evidence from clinopyroxenes and glasses in ultramafic xenoliths of Grande Comore, Indian Ocean. J Petrol 40:133–165

Coulson AL (1933) Barytes in ceded districts of madras presidency, with notes on its occurrence in other parts of India. Mem Geol Surv India 64(Part 1):114–115

Dasgupta R, Hirschmann MM, McDonough WF, Spiegelman M, Withers AC (2009) Trace element partitioning between garnet lherzolite and carbonatite at 6.6 and 8.6 GPa with applications to the geochemistry of mantle and mantle-derived melts. Chem Geol 262:57–77

Davies GR, Stolz AZ, Mahotkin IL, Mowell GM, Pearson DG (2006) Trace element and Sr-Pb-Nd-Hf evidence for ancient, fluid-dominated enrichment of the source of Aldan shield lamproites. J Petrol 47:1119–1146

Deb M, Pal T (2014) Mineral potential of Proterozoic intra-cratonic basins in India. Geol Soc Lond Mem 42:309–325

Drury SA (1984) A Proterozoic intracratonic basin, dyke swarms and thermal evolution in South India. J Geol Soc India 25:437–444

Edgar AD, Vukadinovic D (1992) Implications of experimental petrology to the evolution of ultrapotassic rocks. Lithos 28:205–220

Ersoy YE, Palmer MR, Uysal I, Gundogan I (2014) Geochemistry and petrology of the Early Miocene lamproites and related volcanic rocks in the Thrace Basin, NW Anatolia. J Volcanol Geothem Res 283:143–158

Evenssen NM, Hamilton PJ, O'Nions RK (1978) Rare earth abundances in chondritic meteorites. Geochim Cosmochim Acta 42:1199–1212

Foley SF (1992) Vein-plus-wall-rock melting mechanisms in the lithosphere and the origin of potassic alkaline magmas. Lithos 28:435–438

Foley SF (1993) An experimental study of olivine lamproite: first results from the diamond stability field. Geochim Cosmochim Acta 57: 483–489

Foley SF, Venturelli G, Green DH, Toscani L (1987) The ultra-potassic rocks: characteristics, classification and constraints for petrogenetic models. Earth Sci Rev 24:81–134

Foley SF, Link K, Tiberindwa JV, Barifaijo E (2012) Patterns and origins of igneous activity around the Tanzanian craton. J Afr Earth Sci 62: 1–18

French JE, Heaman LM, Chacko T, Srivastava RK (2007) 1891–1883 Ma Southern Bastar-Cuddapah mafic igneous events, India: a newly recognised large igneous province. Precambrian Res 160:308–322

Fritschle T, Prelević D, Foley SF, Jacob DE (2013) Petrological characterization of the mantle source of Mediterranean lamproites: indications from major and trace elements of phlogopite. Chem Geol 353: 267–279

Gale GH, Dabek LB, Fedikow MAF (1997) The application of rare earth element analyses in the exploration for volcanogenic massive sulfide type deposits. Explor Min Geol 6:233–252

Garza AO, Dostal J, Keppie JD, Moreno FAP (2013) Mid-Tertiary (25–21 Ma) lamprophyres in NW Mexico derived from subduction-modified subcontinental lithospheric mantle in an extensional backarc environment following steepening of the Benioff zone. Tectonophys 590:59–71

Geological Survey of India (2011) Detailed information dossier on diamond in India. 136p

Gibson SA, Thompson RN, Leonardos OH, Dickin AP, Mitchell JG (1995) The Late Cretaceous impact of the Trindade mantle plume: evidence from large-volume, mafic, potassic magmatism in SE Brazil. J Petrol 36:189–229

Gibson SA, Malarkey J, Day J (2008) Melt depletion and enrichment beneath the western Kaapvaal Craton: evidence from Finsch peridotite xenoliths. J Petrol 49:1817–1852

Gudfinnsson GH, Presnall DC (2005) Continuous gradations among primary carbonatitic, kimberlitic, melilititic, basaltic, picritic and komatiitic melts in equilibrium with garnet lherzolite at 3–8 GPa. J Petrol 46:1645–1659

Holland TH (1907) Imperial gazetteer of India. 1:50–103

Ionov DA, Bodinier JL, Mukasa SB, Zanetti A (2002) Mechanisms and sources of mantle metasomatism: major and trace element compositions of peridotite xenoliths from Spitsbergen in the context of numerical modelling. J Petrol 43:2219–2259

Jelsma H, Barnett W, Richards S, Lister G (2009) Tectonic setting of kimberlites. Lithos 112:155–165

Joy S, Jelsma HA, Preston RF, Kota S (2012) Geology and diamond provenance of the Proterozoic Banganapalle conglomerates, Kurnool Group, India. Geol Soc Lond Spec Publ 365:197–218

King W (1872) The Kadapah and Karnul formations in the Madras presidency. Mem Geol Surv India 8:244

Kirchenbaur M, Munker C, Schuth S, Garbe-Schonberg D, Marchev P (2012) Tectonomagmatic constraints on the sources of eastern Mediterranean K-rich lavas. J Petrol 53:27–65

Konzett J, Sweeney RJ, Thompson AB, Ulmer P (1997) Potassium amphibole stability in the upper mantle: an experimental study in a peralkaline KNCMASH system to 8.5 GPa. J Petrol 38:537–568

Krishna Brahmam N, Dutt NVBS (1992) A meteoritic impact theory for the initiation of the Cuddapah (Proterozoic) basin of India. Bull Indian Geol Ass 25:43–60

Kullerud K, Zozulya D, Bergh SG, Hansen H, Ravna EJK (2011) Geochemistry and tectonic setting of a lamproite dyke in Kvaloya, North Norway. Lithos 126:278–289

Kumar A, Gopalan K, Rao KRP, Nayak SS (2001) Rb-Sr ages of kimberlites and lamproites from Eastern Dharwar craton, South India. J Geol Soc India 58:135–142

Kumar KV, Frost CD, Frost BR, Chamberlain BR (2007) The Chimakurthi, Errakonda, and Uppalapadu plutons, Eastern Ghats belt, India: an unusual association of tholeiitic and alkaline magmatism. Lithos 97:30–57

Le Roex AP, Bell DR, Davis P (2003) Petrogenesis of Group I kimberlites from Kimberley, South Africa: evidence from bulk rock geochemistry. J Petrol 44:2261–2286

Lehmann B, Mainkar D, Belyatsky B (2006) The Tokapal crater-facies kimberlite system, Chattisgarh, India: reconnaissance petrography and geochemistry. J Geol Soc India 68:9–18

Lehmann B, Storey C, Mainkar D, Jeffries T (2007) In-situ U-Pb dating of titanite in the Tokapal-Bejripadar kimberlite system, Central India. J Geol Soc India 69:553–556

Madhavan V, Mallikharjuna Rao J, Srinivas M, Natarajan R, Sayeed A (1994) Petrology and petrogenesis of syenites from the Cuddapah basin, Andhra Pradesh. J Geol Soc India 43:225–237

Mall DM, Pandey OP, Chandrakala K, Reddy PR (2008) Imprints of a Proterozoic tectonothermal anomaly below the 1.1 Ga kimberlitic province of the Southwest Cuddapah basin, Dharwar craton (South India). Geophys J Int 172:422–438

Mallikharjuna Rao J, Bhattacharji S, Rao MN, Wampler JM (2007) Potassium-argon ages and geochemical characters of some basic igneous rocks of Cuddapah basin. J Geol Soc India 69:161–170

Masun K, Sthapak AV, Singh A, Vaidya A, Krishna C (2009) Exploration history and geology of the diamondiferous ultramafic Saptarshi intrusions, Madhya Pradesh, India. Lithos 112:142–154

McKenzie D (1985) Extraction of the magma from crust and the mantle. Earth Planet Sci Lett 74:81–91

McKenzie D (1989) Some remarks on the movement of small melt fractions in the mantle. Earth Planet Sci Lett 95:53–72

Meert JG (2012) What's in a name? The Columbia (Palaeopangea/Nuna) Supercontinent. Gondwana Res 21:987–993

Mirnejad H, Bell K (2006) Origin and source evolution of the Leucite Hills lamproites: evidence from Sr-Nd-Pb-O isotopic compositions. J Petrol 47:2463–2489

Mitchell RH (1995) Kimberlites, orangeites and related rocks. Plenum Press, New York

Mitchell RH (2006) Potassic magmas derived from metasomatised lithospheric mantle: nomenclature and relevance to exploration for diamond-bearing rocks. J Geol Soc India 67:317–327

Mitchell RH, Bergman SC (1991) Petrology of lamproites. Plenum Press

Mitchell RH, Edgar AD (2002) Melting experiments on SiO_2-rich lamproites to 6.4 GPa and their bearing on the sources of lamproite magmas. Mineral Petrol 74:115–128

Mitchell RH, Fareeduddin (2009) Mineralogy of peralkaline lamproites from the Raniganj Coalfield, India. Mineral Mag 73:457–477

Mohanty S (2011) Palaeoproterozoic assembly of the Napier Complex, Southern India and Western Australia: implications for the evolution of the Cuddapah basin. Gondwana Res 20:344–361

Murphy DT, Collerson KD, Kamber BS (2002) Lamproites from Gaussberg, Antarctica: possible transition zone melts of Archaean subducted sediments. J Petrol 43:981–1001

Nagaraja Rao BK, Rajurkar ST, Ramalingaswamy G, Ravindra Babu B (1987) Stratigraphy, structure and evolution of the Cuddapah Basin. Geol Soc India Mem 6:33–86

Naqvi SM, Rogers JJW (1987) Precambrian geology of India. Oxford University Press

Nelson DR (1992) Isotopic characteristics of potassic rocks—evidence for the involvement of subducted sediments in the magma. Lithos 28:403–420

Osborne I, Sherlock S, Anand M, Argles T (2011) New Ar-Ar ages of southern Indian kimberlites and a lamproite and their geochemical evolution. Precambrian Res 189:91–103

Palme H, O'Neill HSC (2003) Cosmochemical estimates of mantle composition. In: Holland H, Turekian KK, (eds) Treatise on geochemistry 2: 1–38

Paton C, Hergt JM, Woodhead JD, Phillips D, Shee SR (2009) Identifying the asthenospheric component of kimberlite magmas from the Dharwar craton, India. Lithos 112:296–310

Patranabis-Deb S, Saha D, Tripathy V (2012) Basin stratigraphy, sea-level fluctuations and their global connections: evidence from the Proterozoic Cuddapah Basin. Geol J 47:263–283

Paul DK, Crocket JH, Reddy TAK, Pant NC (2007) Petrology and geochemistry including Platinum Group element abundances of the Mesoproterozoic ultramafic (lamproite) rocks of Krishna district, southern India: implications for source rock characteristics and ptrogenesis. J Geol Soc Indi 69:577–596

Pe-Piper G, Zhang Y, Piper DJW, Prelevic D (2014) Relationship of Mediterranean type lamproites to large shoshonite volcanoes, Miocene of Lesbos, NE Aegean Sea. Lithos 184–187:281–299

Prelević D, Akal C, Foley SF, Romer RL, Stracke A, Bogaard PVD (2012) Ultrapotassic mafic rocks as geochemical proxies for post-collisional dynamics of orogenic lithospheric mantle: the case of Southwestern Anatolia, Turkey. J Petrol 55:1019–1055

Priestly K, McKenzie D (2006) The thermal structure of the lithosphere from shear wave velocities. Earth Planet Sci Lett 244:285–301

Radhakrishna BP (2007) Diamond exploration in India: retrospect and prospect. J Geol Soc of India 69:419–442

Reddy NS (1988) Pillowed spilitic lavas from the Tadpatri formation of the Cuddapah Basin. J Geol Soc of India 32:65–67

Reider M, Cavazzini D, Yakonov YSD, Frank-Kamenetskii VA, Gottardi G, Guggenheim S, PV K, Muller G, Neiva AMR, Radoslovich EW, Robert JL, Sassi FP, Takeda H, Weiss Z, Wones DR (1998) Nomenclature of micas. Can Mineral 36:905–912

Rogers JJW, Santosh M (2009) Tectonics and surface effects of the supercontinent Columbia. Gondwana Res 15:373–380

Saha D, Tripathy V (2012) Tuff beds in Kurnool subbasin, southern India and implications for felsic volcanism in Proterozoic intracratonic basins. Geosci Front 3:429–444

Sahu N, Gupta T, Patel SC, Khuntia DBK, Behera D, Pande K, Das SK (2013) Petrology of lamproites from the Nuapada lamproite field, Bastar craton, India. In: Pearson DG et al (ED) Proceedings of the X International Kimberlite Conference, Bangalore. J Geol Soc India Spec 1: 137–165

Sastry CA, Rama Rao G, Prasad GJS, Reddy VA (2005) Electron micro analysis of indicator minerals from kimberlites of Andhra Pradesh and Karnataka-basic data. Geol Surv India Bull Ser C6:282

Sato K, Katsura T, Ito E (1997) Phase relations of natural phlogopite with and without enstatite up to 8 GPa: implication for mantle metasomatism. Earth Planet Sci Lett 146:511–526

Sen SN, Narasimha Rao H (1971) Chelima dykes—a source for diamonds in Kurnool district, A.P. Geol Surv India Misc Publ 19:92–94

Sesha Sai VV (2014) Pyroclastic volcanism in Papaghni sub-basin, Andhra Pradesh: significant Paleoproterozoic tectonomagmatic event in SW Part of the Cuddapah basin, Eastern Dharwar Craton. J Geol Soc India 83:355–362

Sheppard S, Taylor WR (1992) Barium- and LREE-rich, olivine-mica-lamprophyres with affinities to lamproites, Mt. Bundey, Northern Territory, Australia. Lithos 28:303–325

Singh AP, Mishra DC (2002) Tectonosedimentary evolution of Cuddapah Basin and Eastern Ghats Mobile belt (India) as Proterozoic collision: gravity, seismic and geodynamic constraints. J Geodyn 33:249–267

Srikantia SV (1984) Kuppalapalle volcanic—a distinct Upper Papaghni volcanic activity in the Cuddapah Basin. J Geol Soc India 25:775–779

Sun Y, Ying J, Zhou X, Shao J, Chu Z, Su B (2014) Geochemistry of ultrapotassic volcanic rocks in Xiaogulihe NE China: implications for the role of ancient subducted sediments. Lithos 208–209:53–66

Tainton KM, McKenzie D (1994) The generation of kimberlites, lamproites and their source rocks. J Petrol 35:787–817

Tappe S, Jenner GA, Foley SF, Heaman L, Besserer D, Kjarsgaard BA, Ryan B (2004) Torngat ultramafic lamprophyres and their relation to the North Atlantic Alkaline Province. Lithos 76:491–518

Tappe S, Foley SF, Kjarsgaard BA, Romer RL, Heaman LM, Stracke A, Jenner GA (2008) Between carbonatite and lamproite - diamondiferous Torngat ultramafic lamprophyres formed by carbonate fusion melting of cratonic MARID type metasomes. Geochim Cosmochim Acta 72:3258–3286

Tappe S, Pearson DG, Nowell GM, Nielsen TFD, Milstead P, Muehlenbachs K (2011) A fresh isotopic look at Greenland kimberlites: cratonic mantle lithosphere imprint on deep source signal. Earth Planet Sci Lett 305:235–248

Tappe S, Pearson DG, Kjarsgaard BA, Nowell G (2013) Mantle transition zone input to kimberlite magmatism near a subduction zone: origin of anomalous Nd-Hf isotope systematics at Lac de Gras, Canada. Earth Planet Sci Lett 371–372:235–25

Torsvik TH, Burke K, Steinberger B, Webb SJ, Ashwal LD (2010) Diamonds sampled by plumes from the core–mantle boundary. Nature 466:352–355

Tripathy V, Saha D (2013) Plate margin paleostress variations and intracontinental deformations in the evolution of the Cuddapah basin through Proterozoic. Precambrian Res 235:107–130

Upadhyay D, Raith MM, Mezger K, Hammerschmidt K (2006) Mesoproterozoic rift-related alkaline magmatism at Elchuru, Prakasam Alkaline Province, SE India. Lithos 89:447–477

Wang B, Chen JL, Xu JF, Wang LQ (2014) Geochemical and Sr–Nd–Pb–Os isotopic compositions of Miocene ultrapotassic rocks in southern Tibet: Petrogenesis and implications for the regional tectonic history. Lithos 208–209:237–250

Weyer S, Munker C, Mezger K (2003) Nb/Ta, Zr/Hf and REE in the depleted mantle: implications for the differentiation history of the crust-mantle system. Earth Planet Sci Lett 205:309–324

Yilmaz K (2010) Origin of anorogenic 'lamproite-like' potassic lavas from the Denizli region in Western Anatolia Extensional Province, Turkey. Mineral Petrol 99:219–239